bioRxiv preprint doi: https://doi.org/10.1101/2020.09.01.277707; this version posted September 2, 2020. The copyright holder for this preprint (which was not certified by peer review) is the author/funder, who has granted bioRxiv a license to display the preprint in perpetuity. It is made available under a CC-BY 4.0 International license.

Root growth responses to mechanical impedance are regulated by a network of ROS, ethylene and auxin signalling in Arabidopsis

Amy G.R. Jacobsen[1], Jian Xu[2,3], Jennifer F. Topping[1], Keith Lindsey[1*]

[1]Department of Biosciences, Durham University, Durham DH1 3LE, UK

[2]Department of Plant Systems Physiology, Institute for Water and Wetland Research, Radboud University, Heyendaalseweg 135, 6525 AJ, Nijmegen, The Netherlands

[3]Department of Biological Sciences and Centre for BioImaging Sciences, National University of Singapore, Singapore, 117543, Singapore

[*]Author for correspondence

Tel: +44 191 334 1309

Email: keith.lindsey@durham.ac.uk

Key words: *Arabidopsis thaliana*, auxin, ethylene, mechanical impedance, reactive oxygen species, root growth.

Word count

Summary: 181
Introduction: 1044
Material & Methods: 1313
Results: 2861
Discussion: 1147
Text total: 6365
8 main Figures (all colour), 14 Supplementary Figures, 2 Supplementary Tables.

bioRxiv preprint doi: https://doi.org/10.1101/2020.09.01.277707; this version posted September 2, 2020. The copyright holder for this preprint (which was not certified by peer review) is the author/funder, who has granted bioRxiv a license to display the preprint in perpetuity. It is made available under a CC-BY 4.0 International license.

Summary

- The growth and development of root systems, essential for plant performance, is influenced by mechanical properties of the substrate in which the plants grow. Mechanical impedance, such as by compacted soil, can reduce root elongation and limit crop productivity.
- To understand better the mechanisms involved in plant root responses to mechanical impedance stress, we investigated changes in the root transcriptome and hormone signalling responses of Arabidopsis to artificial root barrier systems *in vitro*.
- We demonstrate that upon encountering a barrier, reduced Arabidopsis root growth and the characteristic 'step-like' growth pattern is due to a reduction in cell elongation associated with changes in signalling gene expression. Data from RNA-sequencing combined with reporter line and mutant studies identified essential roles for reactive oxygen species, ethylene and auxin signalling during the barrier response.
- We propose a model in which early responses to mechanical impedance include reactive oxygen signalling that is followed by integrated auxin and ethylene responses to mediate root growth changes. Inhibition of ethylene responses allows improved growth in response to root impedance, a result that may inform future crop breeding programmes.

Introduction

When growing through soils, plant roots must be able to respond to a range of environmental cues and rely on flexible growth to adapt to changing conditions. Establishment of robust root growth and adaptive root architecture is important for maintaining crop yields, and hence root traits are of interest to plant breeders (Gewin, 2010). Various stress conditions in soils limit root elongation, including insufficient nutrients, oxygen or water, and physical barriers (Bengough *et al*., 2006). As plant roots navigate the soil environment, they encounter physical barriers and must be able to adapt their growth in order to respond mechanical impedance. An increase in the mechanical strength of soils can occur as a result of drying and drought conditions, as there is a strong interaction between soil strength and water content (Whalley *et al*., 2005; Jin *et al*., 2013). The effect of increasing mechanical strength can be further exacerbated by soil compaction caused through the use of heavy farming machinery (Jin *et al*., 2013). Penetrometer resistance is commonly used as a measure of soil strength, and increased

bioRxiv preprint doi: https://doi.org/10.1101/2020.09.01.277707; this version posted September 2, 2020. The copyright holder for this preprint (which was not certified by peer review) is the author/funder, who has granted bioRxiv a license to display the preprint in perpetuity. It is made available under a CC-BY 4.0 International license.

resistance correlates with reduced root elongation (Whitmore & Whalley, 2009; Bengough *et al*., 2011).

Mechanical impedance of the root also affects aerial growth. When roots are mechanically impeded shoot growth slows (Iijima & Kono, 1991; Roberts *et al*., 2002; Kobaissi *et al*., 2013; Potocka & Szymanowska-Pulka, 2018), and changes to leaf growth and morphology are also reported. Leaf number (Grzesiak, 2009), area (Alexander & Miller, 1991; Bingham *et al*., 2010; Kobaissi *et al*., 2013) and elongation rates (Young *et al*., 1997) decrease and stomatal closure has been observed (Roberts *et al*., 2002). There is therefore an agronomic relevance to understanding the response of roots to mechanical impedance, as the effects of soil drying and compaction can reduce crop yields (Whalley *et al*., 2008).

A diverse range of methods have been used to investigate the effect physically constraining root growth has on the morphology and architecture of root systems (Potocka & Szymanowska-Pulka, 2018), and many studies have focused predominantly on the morphological effect of mechanical impedance and barriers to root growth in crop species. It has previously been demonstrated that an increase in soil strength results in a decrease in root elongation in cotton (Taylor & Ratliff, 1969), maize (Bengough & Mullins, 1991), pea (Croser *et al*., 1999; Iijima & Kato, 2007) and tobacco (Alameda *et al*., 2012). In addition studies have demonstrated that in response to mechanical impedance, cell length is reduced and the length of the elongation zone shortened (Veen, 1982; Croser *et al*., 1999; Hanbury & Atwell, 2005; Okamoto *et al*., 2008). The slowed rate of elongation that occurs in mechanically impeded roots is therefore likely to be due to a reduced rate of cell elongation, as axial tension is increased by stiffening of the cell walls to reduce elongation (Bengough *et al*., 2006).

More recently, studies have begun focusing on the response of *Arabidopsis thaliana* in order to investigate in more detail the molecular basis of the root response to mechanical stimulus (Massa & Gilroy, 2003; Okamoto *et al*., 2008; Monshausen *et al*., 2009; Lee *et al*., 2020). Previous studies have sought to investigate the role of plant hormones and signalling pathways in roots in response to touch stimuli or mechanical impedance, however the exact nature of the signalling mechanism remains unknown. Evidence exists that both ethylene and auxin are likely to be involved in mediating the root response to mechanical impedance (Masle, 2002; Braam, 2005; Okamoto *et al*., 2008; Yamamoto *et al*., 2008; Lee *et al*., 2020). Changes in root morphology in mechanically impeded roots often resembles changes observed when roots are exposed to ethylene, an inhibition of root elongation and increase in the proliferation of root hairs (Masle, 2002; Buer *et al*., 2003). Classic studies have examined the response of roots to inclined, hard agar plates (1.5% as opposed to 1%) in order to examine thigmotropic

bioRxiv preprint doi: https://doi.org/10.1101/2020.09.01.277707; this version posted September 2, 2020. The copyright holder for this preprint (which was not certified by peer review) is the author/funder, who has granted bioRxiv a license to display the preprint in perpetuity. It is made available under a CC-BY 4.0 International license.

responses in roots. Roots exhibit a wavy growth pattern due to the mechanical stimulus avoidance response (Okada & Shimura, 1990), and Buer *et al*. (2003) demonstrated that ethylene modulates this response. When Arabidopsis is grown in medium consisting of a normal layer and a harder layer, the root can show a bending response at the lower, harder layer. The bending or non-bending response of roots has been shown to depend on ethylene (Yamamoto *et al*., 2008). The role of ethylene signalling has also been demonstrated in continuously mechanically impeded *Arabidopsis* roots (Okamoto *et al*., 2008; Okamoto & Takahashi, 2019). It is possible that ethylene signalling mediates the response of roots to mechanical stress through co-action with auxin. It has previously been demonstrated that the effect of ethylene on root growth is mediated through regulation auxin biosynthesis and localisation of auxin transporters (Růžička *et al*., 2007; Strader *et al*., 2010).

Previous work also demonstrated that roots respond to obstacles through a combination of thigmotropic and gravitropic reactions (Massa & Gilroy, 2003). Auxin signalling has long been demonstrated to be involved in the gravitropic response of roots (Ottenschläger *et al*., 2003; Swarup *et al*., 2005; Muday & Rahman, 2008). It has also been proposed that the dynamic trafficking system of auxin and the auxin transport system in a key element in controlling tropic growth (Friml *et al*., 2002; Blilou *et al*., 2005; Pernisova *et al*., 2016). Three previous studies to study mechanical root impedance effects in Arabidopsis used either continuous mechanical impedance (horizontal root growth across the surface of a dialysis membrane; Okamoto *et al*., 2008) or the impedance of vertical root growth by a glass or metal barriers (Massa & Gilroy, 2003; Lee *et al*., 2020). Massa & Gilroy (2003) implicated barrier sensing via the root cap; Okamoto *et al*. (2008) demonstrated a role for ethylene signalling in inducing growth inhibition and radial thickening of roots; and Lee *et al*. (2020) showed a role for auxin transport via PIN2 to mediate root bending.

To understand better the network of signalling pathways involved the Arabidopsis root response to impedance, we used transcriptional profiling followed by experimental validation of gene expression data, with a focus on signalling pathway genes. We demonstrate that the early response involves an activation of reactive oxygen species (ROS) associated with ethylene and auxin signalling, and show that each is required for the impedance response.

Materials and Methods

Plant Material

bioRxiv preprint doi: https://doi.org/10.1101/2020.09.01.277707; this version posted September 2, 2020. The copyright holder for this preprint (which was not certified by peer review) is the author/funder, who has granted bioRxiv a license to display the preprint in perpetuity. It is made available under a CC-BY 4.0 International license.

Wildtype (WT) *Arabidopsis thaliana* seeds (Columbia (Col-0) ecotype), the auxin signalling mutant *axr1*, transport mutants *aux1-7* and *eir1-4*, and ethylene-insensitive *etr1* and *ein2* were from laboratory stocks. *atrbohF*, *atrobhD* and *atrbohD/F* mutants were from Prof. Alistair Hetherington (University of Bristol, UK). proCYCB1;2::CYCB1:2:GUS (Schnittger *et. al*., 2002) was from lab stocks. HyPer (Belousov *et al*., 2006) was from Prof. Marc Knight (Durham University, UK). DR5rev::3xVENUS-N7 (Brunoud *et al*., 2012) and R2D2 reporter lines (Liao *et al*., 2015) were from the Nottingham Arabidopsis Stock Centre (http://arabidopsis.info/). Seeds were stratified, surface sterilized and seedlings grown on sterile half strength Murashige and Skoog medium (½MS10) with 0.5% (w/v) agar, or 0.3% (w/v) or 1.2% (w/v) Phytagel depending on the assay, as described (Casson *et al*., 2002).

Barrier Assays

We used three different barrier systems: a high density Phytagel (split medium) system, the use of plastic barriers and growth on the surface of a dialysis membrane, as follows.

1. Split medium assay

Seedlings were grown in Magenta vessels (77 mm × 77 mm × 97 mm) containing a lower layer of 1.2% Phytagel ½MS10 medium, and once set, 0.3% Phytagel medium was poured on top. Seeds were placed just below the surface of the medium, to grow through the upper layer before reaching the barrier layer (Fig. S1a).

2. Plastic and dialysis membrane barrier assays

One horizontal barrier impedance system was adapted from Massa & Gilroy (2003). Seeds were grown on vertical plates containing ½MS10 with 0.5% Phytagel. 1 x 2 cm plastic barriers of clear acetate were sterilised in 70% ethanol and at 6 days after germination (DAG) were placed horizontally directly in front of growing root tips (Fig. S1b); control roots had no barriers. For chemical treatments, seedlings were first germinated on standard ½MS10 medium and transferred at 6 DAG to the treatment plates before barrier placement. For some experiments, roots were grown along the surface of a dialysis membrane on the surface of a horizontal agar plate, to provide continuous impedance, as described (Okamoto *et al*. 2008; Fig. S1c).

For root architecture analysis, seedlings were photographed using a Zeiss STEMI SV8 dissecting stereomicroscope (Carl Zeiss, Cambridge, UK). Each growth assay was repeated 3 times with 15 individuals per treatment. All image analysis was carried out using ImageJ, and

bioRxiv preprint doi: https://doi.org/10.1101/2020.09.01.277707; this version posted September 2, 2020. The copyright holder for this preprint (which was not certified by peer review) is the author/funder, who has granted bioRxiv a license to display the preprint in perpetuity. It is made available under a CC-BY 4.0 International license.

lateral root analysis used the Smart Root Plugin (Lobet *et al*., 2011). Root tip angle (RTA) was measured as the angle between the outer root tip and the horizontal barrier (Massa & Gilroy, 2003; Fig. S1d). For root hair length analysis, up to 20 mature root hairs were measured. The ImageJ straight-line tool was used to draw and measure a line from the quiescent centre (QC) to the proximal end of the meristem (defined as the first cell that was twice the length of the immediately preceding cell; González-García *et al*., 2011). Elongation zone size was measured from the end of the meristem to the first indication of emerging root hairs. Time-lapse imaging of roots used a Dino-lite microscope over 12 h, with images captured every 15 min. RTA and root growth was measured in each image from the point at which the root tip made contact with the barrier.

Histochemistry

Histochemical staining of proCYCB1;2::CYCB1:2:GUS activity with clearing in chloral hydrate solution was as described (Topping & Lindsey, 1997). Number of dividing (GUS-positive) cells was calculated using the ImageJ 'Cell Counter' plugin. CellROX Deep Red dye (ThermoFisher, UK) revealed intracellular accumulation of ROS, and has previously been used for plant roots (Kováčik *et al*., 2014; Wright *et al*., 2016). Whole seedlings were stained with 1 µM dye for 30 min then washed twice with sterile distilled H_2O.

Confocal Microscopy

Roots were imaged using a Leica SP5 laser scanning confocal microscope (www.leica-microsystems.com) or Zeiss LSCM 880 (https://www.zeiss.com/- microscopy/int/home.html). Seedlings were fixed in 4% paraformaldehyde (PFA) before clearing with ClearSee (Kurihara *et al*., 2015) and staining with 0.1% (w/v) Calcofluor White for 30 min or unfixed tissues stained with 0.5% (w/v) propidium iodide (PI) solution for 90 s. Images were opened in LAS AF Lite software (v2.63 build 8173) or Zen Lite software. Images were taken from at least six individual roots for each analysis in Image J.

Analysis of reporter fluorescence

The ImageJ polygon tool was used to delineate regions of interest (ROI) in the root tip. Fluorescence was measured either as mean green channel intensity or mean grey value. Mean green channel intensity was calculated in RGB images using the colour histogram tool. For grey values, all channels were exported as separate TIFFS and converted to 32-bit images and mean grey value measured using the 'set measurement' function in ImageJ. ROIs were selected

bioRxiv preprint doi: https://doi.org/10.1101/2020.09.01.277707; this version posted September 2, 2020. The copyright holder for this preprint (which was not certified by peer review) is the author/funder, who has granted bioRxiv a license to display the preprint in perpetuity. It is made available under a CC-BY 4.0 International license.

194 using the ROI analyser tool and an RGB reference image with all channels, subtracting
195 background from the value. For R2D2, reduction of the Venus signal relative to the tdTomato
196 signal is a proxy for auxin accumulation (Liao *et al*., 2015). Separate TIFFS of the Venus and
197 tdTomato channels were exported and converted to 32-bit in ImageJ. The Image Calculator
198 function of ImageJ determined the ratio of Venus to tdTomato signals
199 (https://imagej.nih.gov/ij/docs/menus/process.html#calculator). For HyPer analysis (Belousov
200 *et al*., 2006), images were acquired at 488 nm (green channel) for analysis using Image
201 Calculator. Images of CellROX DeepRed stained roots were obtained using both confocal and
202 brightfield, using the electronically switchable illumination and detection module (ESID).
203 Fluorescence was measured as mean grey value in 32-bit images containing only the DeepRed
204 channel.
205
206 **RNA-sequencing**
207 20 mg of tissue was ground in liquid nitrogen using TissueLyser II (QIAGEN, Manchester,
208 UK) and RNA extracted using the Qiagen ReliaPrepTM RNA Tissue Miniprep System. RNA
209 quality was determined using the NanoDrop ND-1000 spectrophotometer (ThermoFisher
210 Scientific) and Agilent 2200 TapeStation. Libraries were constructed from 100 ng and 1 µg
211 total RNA using the NEBNext UltraTM Directional RNA Library Prep Kit for Illumina for use
212 with the NEBNext Poly(A) mRNA Magnetic Isolation Module (NEB, Hitchin, UK). mRNA
213 was isolated, fragmented and primed, cDNA was synthesised and end prep was performed.
214 NEBNext Adaptor was ligated and the ligation reaction was purified using AMPure XP Beads.
215 PCR enrichment of adaptor ligated DNA was conducted using NEBNext Multiplex Oligos for
216 Illumina (Set 1, NEB#E7335). The PCR reaction was purified using Agencourt AMPure XP
217 Beads. Library quality was then assessed using a DNA analysis ScreenTape on the Agilent
218 Technologies 2200 TapeStation. qPCR was used for sample quantification using NEBNext®
219 Library Quant Kit Quick Protocol Quant kit for Illumina. Samples were diluted to 10 nM. 7 µl
220 of each 10 nM sample was pooled together and all were run on two lanes using an Illumina
221 HiSeq2500 (DBS Genomics facility, Durham University). Approximately 30M unique paired-
222 end 125bp reads were carried per sample. Primers were designed using Primer-BLAST
223 (http://www.ncbi.nlm.nih.gov/tools/primer-blast/) and synthesised by MWG Eurofins
224 (http://www.eurofinsdna.com/).
225 FastQC (https://www.bioinformatics.babraham.ac.uk/projects/fastqc/) was used to
226 assess read quality and Trimmomatic (Bolger *et al*., 2014) was used to cut down and remove
227 low quality reads. Salmon (Patro *et al*., 2017) was used for quasi-mapping of reads against the

bioRxiv preprint doi: https://doi.org/10.1101/2020.09.01.277707; this version posted September 2, 2020. The copyright holder for this preprint (which was not certified by peer review) is the author/funder, who has granted bioRxiv a license to display the preprint in perpetuity. It is made available under a CC-BY 4.0 International license.

AtRTD2-QUASI (Brown *et al*., 2017; Zhang *et al*., 2017) transcriptome and to estimate transcript-level abundances. The tximport R package (Soneson *et al*., 2016) was used to import transcript-level abundance, estimate counts and transcript lengths, and summarise into matrices for downstream analysis in R. Before differential expression analysis, low quality reads were filtered out of the data set. Only genes with a count per million of 0.744 in 6 or more samples were retained. The DESeq2 (Love *et al*., 2014) R package was used to estimate variance-mean dependence in count data and test for differential expression (using the negative binomial distribution model). A padj-value of ≤0.05 and a $\log^2$fold change of ≥0.5 were selected to identify differentially expressed genes (DEGs). The 3D RNA-Seq online App (Guo *et al*., 2019; Calixto *et al*., 2018) was used for independent verification of estimated DEGs and for differential alternative splicing analysis. RNA-seq data are deposited in the Dryad Digital Repository.

Results

The root response to mechanical impedance involves radially asymmetric changes in cell expansion

In preliminary experiments to investigate the response of roots to a mechanical barrier, a two-layer gel system was used. Vertical root growth was established in a layer of soft medium (0.3% Phytagel) before hitting a harder lower layer (1.2% Phytagel), which creates mechanical impedance. Consistent with previous studies, primary root length significantly decreased on encountering the barrier, with median root length reducing from 15.8 mm (IQR = 4.0) to 10.6 mm (IQR = 3.4) (Fig. 1a). Root length between 4-7 days after germination (DAG) was significantly reduced on impedance, with a significant reduction occurring from 5 DAG (8.21 ± 0.24 mm compared to 5.65 ± 0.36 mm; Fig. 1g). The distance of root hair emergence from the root tip was also significantly reduced on encountering a barrier (Fig. 1b; Okamoto *et al*., 2008). The meristem length of impeded roots (7 DAG) was not significantly different to the control (Fig. 1c,e), but the elongation zone length was significantly reduced, from a median of 467 µm (IQR = 132) in the control to 362 µm (IQR = 123) in impeded roots (Fig. 1d,f).

Analysis of CYCB1;2:GUS reporter expression, which marks the G2/M cell cycle transition (Colon-Carmona *et al.*, 1999; Schnittger *et al.*, 2002), showed the number of dividing cells remained unchanged in response to impedance (Fig. S2 a,b). The ratio of dividing cells on the 'left' and 'right' sides of the axial root plane was calculated using the formula exp(|log(left/right)|), which obviates the need to assign left or right sides. This ratio does not

bioRxiv preprint doi: https://doi.org/10.1101/2020.09.01.277707; this version posted September 2, 2020. The copyright holder for this preprint (which was not certified by peer review) is the author/funder, who has granted bioRxiv a license to display the preprint in perpetuity. It is made available under a CC-BY 4.0 International license.

change in impeded roots (Fig. S2c), indicating cell division rate remains constant radially across the meristem. While primary root length was significantly reduced in impeded roots, lateral root density (i.e. number of laterals per length of primary root) increased (Fig. 1h), suggesting a redistribution of resource to lateral roots in response to the barrier.

To examine the short-term (0-24 h) impedance response, seedlings were grown on vertical plates on the gel surface and at 6 DAG plastic barriers were placed horizontally directly in front of the growing roots. Consistent with previous studies (Massa & Gilroy, 2003; Lee *et al*., 2020), roots were found to rapidly bend away from obstacles, forming a 'step-like' growth pattern where the root grows parallel to the obstacle while the root tip maintains contact with the barrier. It is hypothesized that the first bend represents a touch response to the barrier, leading to 'exploration' of the substrate, while the second bend downwards represents a gravitropic response. Root tip angle (RTA) was measured between the leading edge of the root tip and the surface of the barrier, i.e. at the initiation of the second bend (Fig. S3a; Fig. S1d); this provides a measurable 'readout' of the response to mechanical impedance. RTA changed from an average of 93.8° ± 2.20° (0 h) to 120° ±1.25° (180-480 mins; Fig. S3b), detectable within 60 min of the root encountering an obstacle, with a second bend forming between 3 and 4 hours. The rate of bending (ΔRTA/min) was greatest between 15-90 min (Fig. S3c); root growth rate was fairly constant along the barrier (average 0.96 ± 0.14 mm over 480 min; Fig. S3d).

After 6 h, meristem size was unaffected in roots responding to the barrier (Fig. S3e,f) consistent with changes in cell division unlikely to be involved in the early response to a barrier (Fig. S2; Okamato *et al*. 2008). However, the ratio of the length of the elongation zone between the two sides of the root significantly increased in response to a barrier, from a median ratio of 1.01 (IQR = 0.017) to 1.04 (IQR = 0.027), demonstrating asymmetry in cell elongation (Fig. S3g). The average ratio of cell length for the first 8-11 cells of the elongation zone significantly increased in response to a barrier, confirming the asymmetry (Fig. S3h).

Transcriptional analysis reveals specific signalling changes in the impeded root

The results described show mechanical impedance induces reduced root growth and step-like bending due to differential cell elongation, rather than altered meristem activity, enhanced root hair growth and increased lateral root density. To understand better the molecular events in roots under mechanical impedance stress, time-course RNA-sequencing (RNA-seq) was used to identify transcriptional changes for 3 independent biological replicates for control and

bioRxiv preprint doi: https://doi.org/10.1101/2020.09.01.277707; this version posted September 2, 2020. The copyright holder for this preprint (which was not certified by peer review) is the author/funder, who has granted bioRxiv a license to display the preprint in perpetuity. It is made available under a CC-BY 4.0 International license.

294 barrier treatments of 6 DAG roots at 6 h and 30 h after impedance, representing relatively early
295 and late stages of 'two-step' growth responses.
296 Principal component analysis (Fig. S4a) and a heatmap of the 50 most highly expressed
297 genes with clustering across samples (Fig. S4a) show that variation between sample groups is
298 greater than variation within groups. A P-value of <0.05 and Log2 fold change (log^2fc) of >0.5
299 or <-0.5 were selected to identify differentially expressed genes (DEGs) between barrier and
300 control conditions at each time-point (Fig. S5a). 1941 genes were upregulated and 406
301 downregulated at 6 h after barrier placement. Fewer genes were differentially expressed at 30
302 h, with 852 upregulated and 607 downregulated genes (Fig. S5b). 372 genes were differentially
303 expressed at both 6 h and 30 h (Fig. S5c).
304 In an hypothesis-building process, we carried out an unbiased gene ontology (GO)
305 enrichment analysis to interpret the biological functions of genes upregulated and
306 downregulated at each timepoint, and treemaps were generated using data from REVIGO
307 (Supek *et al*., 2011). Results reveal little overlap between GO terms in the response at 6 h
308 versus 30 h after impedance. Of particular interest, there is seen a strong upregulation in genes
309 involved in 'response to stress', the largest supercluster of GO terms, at 6 h (Fig. S6). GO
310 terms that relate to reactive oxygen species (ROS) are enriched, including 'hydrogen peroxide
311 catabolism' and 'reactive oxygen species metabolism'. Also identified was an enrichment in
312 genes involved in 'signalling', 'protein phosphorylation', 'cell communication, 'secondary
313 metabolism' and 'localization'. At 30 h, there is an upregulation of genes involved in mRNA
314 splicing, cellular respiration and ribonucleoprotein complex biogenesis (Fig. S7). In contrast
315 to the response at 6 h, genes involved in 'cell communication', 'signalling' and 'response to
316 stimulus' are downregulated at 30 h (Fig. S7), indicating a switch from the response at 6 h.
317 At 6 h we found that GO terms relating to hormone responses were enriched in
318 upregulated genes (Fig. S8). In contrast, the majority of genes relating to hormone signalling
319 at 30 h are downregulated, consistent with the observation that many stress-related genes are
320 also downregulated after 30 h (Fig. S8). This indicates that hormone-related transcriptional
321 changes principally occur relatively early in the response to mechanical impedance. Although
322 transcriptional upregulation of genes associated with GA and ABA signalling were identified,
323 analysis of RGA:GFP expression (GA signalling) and treatments with fluoridon (for ABA
324 signalling; Rowe *et al*., 2016) provided no further evidence for an essential role for these
325 pathways in the early impedance response (data not shown); further analysis therefore focused
326 on ROS, ethylene and auxin requirements.
327

bioRxiv preprint doi: https://doi.org/10.1101/2020.09.01.277707; this version posted September 2, 2020. The copyright holder for this preprint (which was not certified by peer review) is the author/funder, who has granted bioRxiv a license to display the preprint in perpetuity. It is made available under a CC-BY 4.0 International license.

A role for ROS in the impedance response

ROS have been proposed to act as a rapid wave-like signal during stress responses, mediated by RESPIRATORY BURST OXIDASE HOMOLOG D (RBOHD) activation (Miller *et al*., 2009; Gilroy *et al*., 2014, 2016). GO analysis showed enrichment in terms relating to ROS metabolism. At 6 h there was an upregulation in genes relating to 'reactive oxygen species metabolism' and 'hydrogen peroxide catabolism'. NADPH oxidases (respiratory burst oxidase homologues) are key ROS-producing enzymes and act as molecular 'hubs' during ROS-mediated signalling (Hu *et al*., 2020). Six NADPH oxidase genes are upregulated at 6 h (Table S1), including *RBHOD* and *RBOHF*, which have been shown to be involved in a number of abiotic and biotic stress responses (Xie *et al*., 2011; Liu *et al*., 2015; Morales *et al*., 2016; Wang *et al*., 2019). *ROOT HAIR DEFECTIVE 2* (*RHD2*) is upregulated at 6 h, and has been linked to root hair growth (Foreman *et al*., 2003) and root touch responses (Monshausen *et al*., 2009). In addition, 20 known ROS scavenging genes were upregulated at 6 h (Table S2).

Transcriptomic changes in response to ROS have previously been documented and a transcriptomic footprint created (Gadjev *et al*., 2006). Comparison of this footprint with the data obtained for response to a barrier revealed that, at 6 h, 32 upregulated genes overlap with the ROS footprint (Fig. 2a). The greatest number of DEGs at 6 h appear to be upregulated in response to singlet oxygen (Fig. 2b), strongly suggesting an elevation of ROS transcriptional and signalling responses when a root encounters a barrier.

Since *RBHOD* and *RBOHF* genes were upregulated within 6 h, time-lapse imaging was used to examine the early root response of the *atrbohD/F* double mutant after encountering a barrier (Fig. 3a). The *atrbohD/F* root tip angle differed significantly from Col-0 at 360 min, with mean RTA of *atrbohD/F* of 148.8º (± 5.7) compared with 118.9º (± 8.2) in the control (Fig. 3b; ANCOVA, $p < 0.001$); differences were detected from ca. 75 min. At 75 min the RTA of *atrbohD/F* is greater at 124.0º (± 6.7) compared with 108.9º (±4.4) for Col-0 (Fig. 3b), demonstrating a requirement for these ROS signalling pathway genes in the early impedance response.

Diphenylene iodonium (DPI), a chemical inhibitor of ROS production, was used to investigate further the role of ROS in the barrier response. Seedlings were grown on 10 µM DPI or 10 µM DMSO as a control, and barrier response determined. At 6 h, seedlings grown on 10 µM of DPI encountering a barrier exhibited a higher RTA compared to the control (10 µm DMSO; Fig. 3c), confirming the mutant study. At 24 h, there was no significant difference in RTA between seedlings grown in the presence of 10 µM DPI on 10 µM DMSO when encountering a barrier (Fig. 3d).

bioRxiv preprint doi: https://doi.org/10.1101/2020.09.01.277707; this version posted September 2, 2020. The copyright holder for this preprint (which was not certified by peer review) is the author/funder, who has granted bioRxiv a license to display the preprint in perpetuity. It is made available under a CC-BY 4.0 International license.

Confocal imaging of the H_2O_2 reporter HyPer (Belousov *et al*., 2006) was used to investigate possible changes in H_2O_2 levels at the root tip in response to impedance within 6 h. YFP fluorescence increased significantly in the root cap border cells, indicating an increase in H_2O_2 (Fig. 3e,f). There was no significant change detected in other cells of the root cap (Fig. 3g,h).

CellROX Deep Red is a cell-permeant dye that is weakly fluorescent in the reduced state and exhibits photostable fluorescence upon oxidation by ROS. Three hours after barrier placement, fluorescence was observed in the outermost columella, border cells and in the lateral root cap (Fig. 4a) but was not significantly different in either the columella cells or lateral root cap in the two treatments (Fig. 4b) Fluorescence was also observed in both the meristematic and elongation zones (Fig. 4c), and while there was no difference in meristem cells, there was found a significant decrease in CellROX fluorescence in the elongation zone in roots encountering a barrier (Fig. 4d, Student's *t*-test, $p = 0.05$), indicating a decrease in ROS.

A role for ethylene in the impedance response

KEGG pathway mapping identified upregulation of ethylene-related transcription at 6 h, including key ethylene response genes such as *ETHYLENE INSENSTIVE LIKE 2* (*EIL2*; Fig. S9a) and two *ETHYLENE RESPONSE FACTOR* (*ERF*) genes *ERF1A* and *ERF4*, and genes involved in ethylene biosynthesis - *ACS5* is upregulated by $\log^2$FC of 2.52, and the ACC oxidase gene *ETHYLENE FORMING ENZYME* (*EFE*) is also upregulated at 6 h, suggesting increased ethylene production in response to a barrier (Fig. S9b). At 30 h, *ACS5* and *ELO1* are both downregulated, indicating a possible decrease in ethylene biosynthesis. These data suggest that upregulation in ethylene biosynthesis may be early and transient during the barrier response.

Previous studies describe controversy around a role for ethylene synthesis, and suggested primarily a role for ethylene signalling, in the response to continuous impedance (Okamoto *et al*., 2003). To investigate a possible requirement for ethylene signalling for the root response, time lapse imaging was used to investigate the bending of the ethylene resistant *etr1-1* mutant in response to a barrier (Fig. 5a). RTA changed more rapidly in *etr1*compared with Col-0 in response to a barrier, detectable from ca. 45-60 min, indicating a relatively early role of ethylene signalling in the impedance response. At 60 min, mean RTA of *etr1* was 122.9° ± 3.40, 15.6 degrees higher than the root tip angle of Col-0 (107.3° ± 5.53). The RTA of *etr1* also reduced again toward the vertical between 195 and 270 min, reaching 117.6° ±9.9 at 270 min before increasing again to 150° ±12.9 at 360 min (Fig. 5b,c), associated with the second

bioRxiv preprint doi: https://doi.org/10.1101/2020.09.01.277707; this version posted September 2, 2020. The copyright holder for this preprint (which was not certified by peer review) is the author/funder, who has granted bioRxiv a license to display the preprint in perpetuity. It is made available under a CC-BY 4.0 International license.

bend. *ein2* also showed a slightly more vertical root than wildtype (though not significant at the P<0.05 level; Fig. S10), indicating a role for ethylene signalling in reducing growth rate and bending on impedance. *etr1* seedlings grew longer than wildtype in a gel barrier (Fig. S11) and roots of a range of ethylene-insensitive mutants (*ein2*, *etr1*, *aux1*, *eir1*) were not significantly inhibited by barrier impedance (ANOVA, p<0.0001; Fig. S12).

To further examine the role of ethylene, seedlings were grown in the presence of chemical inhibitors of ethylene biosynthesis (10 µM AVG) and signalling (10 µM silver thiosulphate, STS). At 6 h after barrier placement, seedlings grown in the presence of either inhibitor showed a slightly higher RTA than the control, however this was non-significant (Fig. 5d, ANOVA, p = 0.08). After 24 h of growth, seedlings grown on 10 µM AVG had a significantly higher mean RTA than the control (Fig. 5e; ANOVA, p < 0.001; TUKEY p = 0.003), indicating a role for ethylene synthesis at the later stages of impedance response (likely associated with gravitropism). However, seedlings grown in the presence of STS did not exhibit any significant change in RTA compared with the control (Fig. 5e, TUKEY, p > 0.05).

Root hair density and length were measured in roots responding to a barrier in the presence of 10 µM AVG or STS. At 24 h of barrier treatment, control seedlings showed an increase in root hair length in response to a barrier as described above, which together with root hair density was significantly reduced by treatment with 10 µM AVG or 10 µM STS in either the presence or absence of barrier (Fig. 5f-h; ANOVA, P <0.001). This shows that normal ethylene biosynthesis and signalling are each essential for root hair elongation and formation, but only root hair length increases in response to barrier contact.

A role for auxin in the impedance response

Further KEGG pathway mapping revealed DEGs associated with auxin signalling. At 6 h *PHYTOCHROME-ASSOCIATED PROTEIN 2* (*PAP2*), a member of the *AUXIN/INDOLE-3-ACETIC ACID* (*Aux/IAA*) family, and *SAUR36* are downregulated, while *SAUR55* is upregulated; *SAUR36* is upregulated at 30 h. At 30 h, 3 *AUX/IAA* genes are differentially expressed: *IAA30* and *PAP2* are upregulated while *IAA14* is downregulated (Fig. S13). Three genes involved in auxin conjugation, *GH3.17*, *BRU6* and *DFL1* (Staswick *et al*., 2005) are also upregulated at 6 h and two downregulated at 30 h (*GH3.17* and *DFL2*, Fig. S13), suggesting a role for auxin conjugation in controlling free auxin levels during the barrier response. Three ATP-Binding Cassette (ABC) family genes, *ABCB1*, *ABCB4* and *ABCG37*, associated with auxin transport and gravitropic response (Geisler *et al*., 2005; Wu *et al*., 2007; Lewis *et al*., 2007; Růžička *et al*., 2010) are upregulated at 6 h.

bioRxiv preprint doi: https://doi.org/10.1101/2020.09.01.277707; this version posted September 2, 2020. The copyright holder for this preprint (which was not certified by peer review) is the author/funder, who has granted bioRxiv a license to display the preprint in perpetuity. It is made available under a CC-BY 4.0 International license.

The transcriptomic data presented above, and recent work by Lee *et al*. (2020), support a role for auxin and its transport in obstacle avoidance. Using time lapse imaging, we found that RTA for the auxin transport (and ethylene-insensitive) mutants *eir1-4* and *aux1-7* was significantly closer to the horizontal than Col-0 (Fig. 6a,b), apparent from ca. 210 min (average RTA for *eir1-4* is 133 ± 5.5° and 138.4 ± 3.4° for *aux1-7*, compared with 123.8 ± 2.6° for Col-0). Initial bending between 0 and 210 minutes appears the same between Col-0 and the mutants (Fig. 6b). After 24 h the RTA was still significantly different between Col-0 and the mutants (ANOVA, $P < 0.001$; Fig. 6c). Wildtype seedlings treated with the auxin transport inhibitor N-1-naphthylphthalamic acid (10 µM NPA) at 6 h after barrier interaction had a significantly higher RTA than untreated controls (161 ± 4.4°) (Fig. 6d) and at 24 h mean RTA at both 2.5 and 10 µM NPA was greater than the untreated controls (Fig. 6e).

Mechanical impedance caused a significant increase in fluorescence of the reporter line DR5rev::3xVENUS-N7 tip 6 h after encountering a barrier in the stele and lateral root cap (Fig. 7a,b). Similarly, the ratiometric reporter R2D2 showed Tomato/Venus fluorescence increased significantly at 6 h (Fig. 7c-e), indicating an increase in auxin levels. Asymmetric distribution of auxin was also detected, with 'left to right' auxin level increasing significantly in response to impedance (Fig. 7d). There was also a significant increase in Tomato/Venus fluorescence by 4 h, i.e. the time when auxin transport mutants showed altered RTA responses (ANOVA $p = 0.001$, Fig. S14), indicating a significant increase in auxin at the root tip in that early response period. Cell type analysis also revealed a significant change in left/right auxin level in the LRC/Epidermis between 2 h and 4 h (ANOVA, $p = 0.03$; Fig. S14). These data show auxin distribution dynamics across the root occurring at early time points from the first bending impedance response.

Discussion

Previous studies have investigated the response of roots to mechanical stimulation through the use of artificial obstacles to growth or changes in orientation of growing roots. Alterations in root system morphology are observed when a plant is reoriented with respect to the direction of the gravitational field. For example, *Arabidopsis* roots produce a characteristic wavy growth pattern when grown on tilted agar plates with impenetrable surfaces (Okada & Shimura, 1990; Rutherford & Masson, 1996). These patterns of growth are the result of a combination of gravity sensing and touch stimulation from the agar surface (Oliva & Dunand, 2007).

bioRxiv preprint doi: https://doi.org/10.1101/2020.09.01.277707; this version posted September 2, 2020. The copyright holder for this preprint (which was not certified by peer review) is the author/funder, who has granted bioRxiv a license to display the preprint in perpetuity. It is made available under a CC-BY 4.0 International license.

Placing a horizontal obstacle in the way of a vertically growing root reveals another pattern of growth likely to be induced by a combination of touch sensing and gravity, the barrier response. When encountering a barrier, *Arabidopsis* roots show a 'step-like' growth, with only the root tip remaining in contact with the barrier surface (Massa & Gilroy, 2003; Lee et al., 2020). Root bending has also been observed in roots grown in a medium consisting of a soft upper layer and a hard lower layer. The root exhibits a bending response at the lower, harder layer (Yamamoto *et al*., 2008; Yan *et al*., 2017, 2018). It has been suggested that a zone of 'mechanical weakness' is required for the bending process and that this is localised between the growing and mature zones of the root (Bizet *et al*., 2016).

While the tropic responses of roots have been characterized in different substrates with different mechanical barrier properties, there is limited information on the molecular responses and controlling mechanisms. The first bend, on touching the barrier, is likely a touch response mediated, it has been suggested, by cells of the root cap (Massa & Gilroy, 2003) followed by a gravitropic response to keep the root tip pointing downwards while the elongation of the root causes lateral movement; this response appears to require polar auxin transport via PIN2 (Lee *et al*., 2020).

In our system, we similarly observed the two-step growth pattern, and the RNA-seq analysis revealed significant changes in three, likely inter-related, signalling pathways, namely ROS, ethylene and auxin. From an analysis of the RTA of ROS, ethylene signalling and auxin transport mutants and reporter imaging studies, it would appear that ROS and ethylene responses occur relatively early, during the period of the touch and first bend of the root, followed by auxin responses. The root behaviour of the *atrbohD/F* double mutant, defective in ROS generation, is first detectable within ca. 75 min of barrier touching, followed by Hyper and CellROX ROS reporter accumulation in root cap border cells and lateral root cap and root elongation zone within 3 h (Figs. 3 & 4). No significant barrier effect on ROS reporter activity was seen in the root meristem. Early ethylene requirements were also seen as altered root behaviour of the ethylene-insensitive *etr1* mutant within 45-60 min of barrier contact. Over a longer period (6-24 h), a likely role for ethylene biosynthesis was identified through root responses of seedlings (RTA, root hair density and length) treated with the ethylene synthesis inhibitor AVG (Fig. 5). However, our RNA-seq data suggest an upregulation in ethylene signalling and biosynthesis at the transcriptional level is transient. At 30 h, *ACS5* is downregulated and there is no upregulation of any ethylene signalling genes. When ethylene signalling is perturbed, decreases in root growth in response to a barrier are not observed (Okamoto *et al*., 2008; Okamoto & Takahashi, 2019). The Arabidopsis ethylene-insensitive

bioRxiv preprint doi: https://doi.org/10.1101/2020.09.01.277707; this version posted September 2, 2020. The copyright holder for this preprint (which was not certified by peer review) is the author/funder, who has granted bioRxiv a license to display the preprint in perpetuity. It is made available under a CC-BY 4.0 International license.

mutants either grow longer or are less inhibited than wildtype following barrier contact (Figs. S11, S12), suggesting that ethylene signalling may represent a useful target for breeders hoping to improve root growth in compact soils.

Consistent with recent previous work (Lee *et al*., 2020), auxin transport effects were observed through altered bending responses of *aux1* and *eir1* (*pin2*) mutants (which also exhibit ethylene sensitivity) or seedlings treated with the auxin transport inhibitor NPA, but not until after ca. 6-24 h after barrier contact; although auxin-related transcriptional changes were established by 6 h (Fig. 6).

Plant signalling systems act in an interacting network to elicit developmental change, such as in root growth and developmental responses to environmental stresses in the soil (Moore *et al*., 2015; Rowe *et al*., 2016). It is known for example that ethylene can lead to reduced primary root growth in Arabidopsis by activating auxin biosynthesis in the root tip and promoting its transport to the elongation zone, where it inhibits cell elongation (Ruzicka *et al*., 2007; Swarup *et al*., 2007). Given this evidence, and the observed timing of ethylene and auxin responses on contact with a mechanical barrier, it seems likely that ethylene signalling and/or synthesis changes lead to altered root growth and bending by effects on auxin distribution, as seen in Figs. 7 & 8. It is also likely that PIN2 is involved in the observed auxin redistribution (Lee *et al*. 2020), though other PIN proteins, AUX1, and possibly ABC transporters may also be involved. The activation of root hair development in response to barrier contact may represent a mechanism to anchor the root in the soil to facilitate the observed lateral growth around the barrier, as part of the soil exploration process.

An interesting question is around the role of ROS. The evidence presented shows a relatively rapid upregulation of ROS-related gene transcription, including of genes encoding ROS-generating enzymes such as RHD2, required for root hair development and other stress responses (Foreman *et al*., 2003). What is unclear at present is the mechanistic relationship between ROS production and the activity of other signalling pathways, such as ethylene and auxin (Fig. 8). Inhibition of ROS signalling, such as in the *atrbohD/F* mutant or following treatment with the ROS inhibitor DPI, led to early changes in the root response to mechanical impedance, but how this might in turn lead to an activation of ethylene signalling (which in turn can induce auxin synthesis and transport) remains to be discovered. Monshausen *et al*. (2009) have demonstrated that ROS production in response to mechanical stimuli requires Ca^{2+} signalling. ROS and Ca^{2+} have been proposed to act together, with NADPH oxidase-produced ROS activating Ca^{2+} channels and the increase in Ca^{2+}, in turn further activating NADPH

bioRxiv preprint doi: https://doi.org/10.1101/2020.09.01.277707; this version posted September 2, 2020. The copyright holder for this preprint (which was not certified by peer review) is the author/funder, who has granted bioRxiv a license to display the preprint in perpetuity. It is made available under a CC-BY 4.0 International license.

oxidase activity (Gilroy *et al*., 2016). Recently, Wu *et al*. (2020) identified the first H_2O_2 receptor in plants, HPCA1. This membrane bound receptor kinase was also shown to mediate H_2O_2-induced activation of Ca^{2+} channels in guard cells, providing further evidence for how ROS mediates Ca^{2+} signalling. Data from our RNA-seq at 6 h after barrier contact did reveal an upregulation of this gene, three related genes (*HPCAL1, HPCAL2*, *HPCAL4*) and also genes involved in Ca^{2+} signalling, binding and transport, suggesting changes in levels of Ca^{2+} in the root. Future work should aim to explore further the interactions between ROS and Ca^{2+}, and auxin and ethylene signalling during the root barrier response.

Acknowledgements

KL acknowledges The Biotechnology and Biological Sciences Research Council (BBS/B/0773X) and Durham University for funding.

Author contributions

KL and JFT devised the project; AGRJ carried out the experimental work; KL, JFT, and JX supervised the work; KL and AGRJ drafted the manuscript; all authors edited the manuscript.

Data availability statement

All materials and data described in this paper are available to readers from the corresponding author, upon reasonable request.

References

Alameda D, Anten NP, Villar R. 2012. Soil compaction effects on growth and root traits of tobacco depend on light, water regime and mechanical stress. *Soil and Tillage Research* **120**: 121–129.

Alexander KG, Miller MH. 1991. The effect of soil aggregate size on early growth and shoot-root ratio of maize (Zea mays L.). *Plant and Soil* **138**: 189– 194.

Belousov VV, Fradkov AF, Lukyanov KA, Staroverov DB, Shakhbazov KS, Terskikh AV, Lukyanov S. 2006. Genetically encoded fluorescent indicator for intracellular hydrogen peroxide. *Nature Methods* **3**: 281–286.

Bengough AG, Bransby MF, Hans J, McKenna SJ. Roberts TJ, Valentine TA. 2006. Root responses to soil physical conditions; growth dynamics from field to cell. *Journal of Experimental Botany* **57**: 437–447.

bioRxiv preprint doi: https://doi.org/10.1101/2020.09.01.277707; this version posted September 2, 2020. The copyright holder for this preprint (which was not certified by peer review) is the author/funder, who has granted bioRxiv a license to display the preprint in perpetuity. It is made available under a CC-BY 4.0 International license.

562 **Bengough AG, McKenzie BM, Hallett PD, Valentine TA. 2011.** Root elongation, water
563 stress, and mechanical impedance: A review of limiting stresses and beneficial root tip traits.
564 *Journal of Experimental Botany* **62**: 59–68.
565 **Bengough AG, Mullins CE. 1991.** Penetrometer resistance, root penetration resistance and
566 root elongation rate in two sandy loam soils. *Plant and Soil* **131**: 59–66.
567 **Bingham IJ, Bengough AG, Rees RM. 2010.** Soil compaction-N interactions in barley: Root
568 growth and tissue composition. *Soil and Tillage Research* **106**: 241–246.
569 **Bizet F, Bengough AG, Hummel I, Bogeat-Triboulot MB, Dupuy LX. 2016.** 3D
570 deformation field in growing plant roots reveals both mechanical and biological responses
571 to axial mechanical forces. *Journal of Experimental Botany* **67**: 5605–5614.
572 **Blilou I, Xu J, Wildwater M, Willemsen V, Paponov I, Friml J, Heldstra R, Aida M,**
573 **Palme K, Scheres B. 2005.** The PIN auxin efflux facilitator network controls growth and
574 patterning in Arabidopsis roots. *Nature* **433**: 39– 44.
575 **Bolger AM, Lohse M, Usadel B. 2014.** Trimmomatic: A flexible trimmer for Illumina
576 sequence data. *Bioinformatics* **30**: 2114–2120.
577 **Braam J. 2005.** In touch: Plant responses to mechanical stimuli. *New Phytologist* **165**: 373–
578 389.
579 **Brown JW, Calixto CP, Zhang R. 2017.** High-quality reference transcript datasets hold the
580 key to transcript-specific RNA-sequencing analysis in plants. *New Phytologist* **213**: 525–
581 530.
582 **Brunoud G, Wells DM, Oliva M, Larrieu A, Mirabet V, Burrow AH, Beeckman T,**
583 **Kepinski S, Traas J, Bennett MJ, Vernoux T. 2012.** A novel sensor to map auxin response
584 and distribution at high spatio-temporal resolution. *Nature* **482**: 103–106.
585 **Buer CS, Wasteneys GO, Masle J. 2003.** Ethylene modulates root-wave responses in
586 Arabidopsis. *Plant Physiology* **132**: 1085–1096.
587 **Calixto CP, Guo W, James AB, Tzioutziou NA, Entizne JC, Panter PE, Knight H, Nimmo**
588 **HG, Zhang R, Brown JW. 2018.** Rapid and dynamic alternative splicing impacts the
589 arabidopsis cold response transcriptome. *Plant Cell* **30**: 1424–1444.
590 **Casson SA, Chilley PM, Topping JF, Evans I., Souter MA, Lindsey K. 2002.** The *POLARIS*
591 gene of Arabidopsis encodes a predicted peptide required for correct root growth and leaf
592 vascular patterning. *Plant Cell* **14**: 1705–1721.
593 **Colon-Carmona A, You R, Haimovitch-Gal T, Doerner P. 1999.** Spatio-temporal analysis
594 of mitotic activity with a labile cyclin-GUS fusion protein. *Plant Journal* **20**: 503–508.

bioRxiv preprint doi: https://doi.org/10.1101/2020.09.01.277707; this version posted September 2, 2020. The copyright holder for this preprint (which was not certified by peer review) is the author/funder, who has granted bioRxiv a license to display the preprint in perpetuity. It is made available under a CC-BY 4.0 International license.

595 **Croser C, Bengough AG, Pritchard J. 1999.** The effect of mechanical impedance on root
596 growth in pea (*Pisum sativum*). I. Rates of cell flux, mitosis, and strain during recovery.
597 *Physiologia Plantarum* **107**: 277–286.
598 **Foreman J, Demidchik V, Bothwell JH, Mylona P, Miedema H, Angel Torres M, Linstead**
599 **P, Costa S, Brownlee C, Jones JD, Davies JM, Dolan L. 2003.** Reactive oxygen species
600 produced by NADPH oxidase regulate plant cell growth. *Nature* **422**: 442–446.
601 **Friml J, Wisniewska J, Benková E, Mendgen K, Palme K. 2002.** Lateral relocation of auxin
602 efflux regulator PIN3 mediates tropism in Arabidopsis. *Nature* **415**: 806–809.
603 **Gadjev I, Vanderauwera S, Gechev TS, Laloi C, Minkov IN, Shulaev V, Apel K, Inzé D,**
604 **Mittler R, Van Breusegem F. 2006.** Transcriptomic footprints disclose specificity of
605 reactive oxygen species signaling in Arabidopsis. *Plant Physiology* **141**: 436–445.
606 **Geisler M, Blakeslee JJ, Bouchard R, Lee OR, Vincenzetti V, Bandyopadhyay A,**
607 **Titapiwatanakun B, Peer WA, Bailly A, Richards EL, Ejendal KF, Smith AP, Baroux**
608 **C, Grossniklaus U, Müller A, Hrycyna CA, Dudler R, Murphy AS, Martinoia E. 2005.**
609 Cellular efflux of auxin catalyzed by the Arabidopsis MDR/PGP transporter AtPGP1. *Plant*
610 *Journal* **44**: 179–194.
611 **Gewin V. 2010.** Food: An underground revolution. *Nature* **466**: 552–553.
612 **Gilroy S, Białasek M, Suzuki N, Górecka M, Devireddy AR, Karpińsk S., Mittler R. 2016.**
613 ROS, calcium, and electric signals: Key mediators of rapid systemic signaling in plants.
614 *Plant Physiology* **171**: 1606–1615.
615 **Gilroy S, Suzuki N, Miller G, Choi WG, Toyota M, Devireddy AR, Mittler R. 2014.** A
616 tidal wave of signals: Calcium and ROS at the forefront of rapid systemic signaling. *Trends*
617 *in Plant Science* **19**: 623–630.
618 **González-García M-P, Vilarrasa-Blasi J, Zhiponova M, Divol F, Mora-García S,**
619 **Russinova E, Caño-Delgado AI. 2011.** Brassinosteroids control meristem size by
620 promoting cell cycle progression in Arabidopsis roots. *Development* **138**: 849–59.
621 **Grzesiak MT. 2009.** Impact of soil compaction on root architecture, leaf water status, gas
622 exchange and growth of maize and triticale seedlings. *Plant Root* **3**: 10–16.
623 **Guo W, Tzioutziou N, Stephen G, Milne I, Calixto C, Waugh R, Brown JW, Zhang R.**
624 **2019.** 3D RNA-seq - a powerful and flexible tool for rapid and accurate differential
625 expression and alternative splicing analysis of RNA-seq data for biologists. *BioRxiv*:
626 656686.
627 **Hanbury CD, Atwell BJ. 2005.** Growth dynamics of mechanically impeded lupin roots: Does
628 altered morphology induce hypoxia? *Annals of Botany* **96**: 913–924.

bioRxiv preprint doi: https://doi.org/10.1101/2020.09.01.277707; this version posted September 2, 2020. The copyright holder for this preprint (which was not certified by peer review) is the author/funder, who has granted bioRxiv a license to display the preprint in perpetuity. It is made available under a CC-BY 4.0 International license.

629 **Hu C-H, Wang P-Q, Zhang P-P, Nie X-M, Li B-B, Tai L, Liu W-T, Li W-Q, Chen K-M.**
630 **2020.** NADPH Oxidases: the vital performers and center hubs during plant growth and
631 signaling. *Cells* **9**: 437.
632 **Iijima M, Kato J. 2007.** Combined soil physical stress of soil drying, anaerobiosis and
633 mechanical impedance to seedling root growth of four crop species. *Plant Production*
634 *Science* **10**: 451–459.
635 **Iijima M, Kono Y. 1991.** Interspecific differences of the root system structures of four cereal
636 species as affected by soil compaction. *Japanese Journal of Crop Science* **60**: 130–145.
637 **Jin K, Shen J, Ashton RW, Dodd IC, Parry MA, Whalley WR. 2013.** How do roots elongate
638 in a structured soil? *Journal of Experimental Botany* **64**: 4761–4777.
639 **Kobaissi A, Kanso, AA, Kanbar HJ, Kazpard VA. 2013.** Morpho-physiological changes
640 caused by soil compaction and irrigation on *Zea mays*. *Eurasian Journal of Soil Science* **2**:
641 114–121.
642 **Kováčik J, Babula P, Hedbavny J, Švec P. 2014.** Manganese-induced oxidative stress in two
643 ontogenetic stages of chamomile and amelioration by nitric oxide. *Plant Science* **215-216**:
644 1–10.
645 **Kurihara D, Mizuta Y, Sato Y, Higashiyama T. 2015.** ClearSee: A rapid optical clearing
646 reagent for whole-plant fluorescence imaging. *Development* **142**: 4168–4179.
647 **Lee HJ, Kim HS, Park JM, Cho HS, Jeon JH. 2020.** PIN- mediated polar auxin transport
648 facilitates root obstacle avoidance. *New Phytologist* **225**: 1285–1296.
649 **Lewis DR, Miller ND, Splitt BL, Wu G, Spalding EP. 2007.** Separating the roles of acropetal
650 and basipetal auxin transport on gravitropism with mutations in two arabidopsis multidrug
651 resistance-like ABC transporter genes. *Plant Cell* **19**: 1838–1850.
652 **Liao CY, Smet W, Brunoud G, Yoshida S, Vernoux T, Weijers D. 2015.** Reporters for
653 sensitive and quantitative measurement of auxin response. *Nature Methods* **12**: 1098.
654 **Liu HB, Wang XD, Zhang YY, Dong JJ, Ma C, Chen WL. 2015.** NADPH oxidase RBOHD
655 contributes to autophagy and hypersensitive cell death during the plant defense response in
656 *Arabidopsis thaliana*. *Biologia Plantarum* **59**: 570–580.
657 **Lobet G, Pagès L, Dray, X. 2011.** A novel image-analysis toolbox enabling quantitative
658 analysis of root system architecture. *Plant Physiology* **157**: 29–39.
659 **Love MI, Huber W, Anders S. 2014.** Moderated estimation of fold change and dispersion for
660 RNA-seq data with DESeq2. *Genome Biology* **15**: 550.

bioRxiv preprint doi: https://doi.org/10.1101/2020.09.01.277707; this version posted September 2, 2020. The copyright holder for this preprint (which was not certified by peer review) is the author/funder, who has granted bioRxiv a license to display the preprint in perpetuity. It is made available under a CC-BY 4.0 International license.

Masle J. 2002. High soil strength: mechanical forces at play on root morphogenesis and in root:shoot signaling. In *Plant Roots: the Hidden Half*, eds. Waisel Y, Amram E, Uzi K, pp. 807–819. Marcel Dekker, NY.

Massa GD, Gilroy S. 2003. Touch modulates gravity sensing to regulate the growth of primary roots of Arabidopsis thaliana. *Plant Journal* **33**: 435–445.

Miller G, Schlauch K, Tam R, Cortes D, Torres MA, Shulaev V, Dangl JL, Mittler R. 2009. The plant NADPH oxidase RBOHD mediates rapid systemic signaling in response to diverse stimuli. *Science Signaling* **2**: ra45.

Monshausen GB, Bibikova TN, Weisenseel MH, Gilroy S. 2009. Ca^{2+} regulates reactive oxygen species production and pH during mechanosensing in arabidopsis roots. *Plant Cell* **21**: 2341–2356.

Moore S, Zhang X, Mudge A, Rowe JH, Topping JF, Liu J, Lindsey K. 2015. Spatiotemporal modelling of hormonal crosstalk explains the level and patterning of hormones and gene expression in *Arabidopsis thaliana* wild-type and mutant roots. *New Phytologist* **207**: 1110–1122.

Morales J, Kadota, Y, Zipfel C, Molina A, Torres MA. 2016. The Arabidopsis NADPH oxidases RbohD and RbohF display differential expression patterns and contributions during plant immunity. *Journal of Experimental Botany* **67**: 1663–1676.

Muday GK, Rahman A. 2008. Auxin Transport and the Integration of Gravitropic Growth. In Gilroy S, Masson P eds., *Plant Tropisms*, pp 47–77. Blackwell, Oxford, England.

Okada K, Shimura,Y. 1990. Reversible root tip rotation in Arabidopsis seedlings induced by obstacle-touching stimulus. *Science* **250**: 274–276.

Okamoto T, Takahashi,T. 2019. Ethylene signaling plays a pivotal role in mechanical-stress-induced root-growth cessation in *Arabidopsis thaliana*. *Plant Signaling and Behavior* **14**: 1669417.

Okamoto T, Tsurumi S, Shibasaki K, Obana Y, Takaji H, Oono Y, Rahman A. 2008. Genetic dissection of hormonal responses in the roots of arabidopsis grown under continuous mechanical impedance. *Plant Physiology* **146**: 1651–1662.

Oliva M, Dunand C. 2007. Waving and skewing: How gravity and the surface of growth media affect root development in Arabidopsis. *New Phytologist* **176**: 37–43.

Ottenschläger I, Wolff P, Wolverton C, Bhalerao RP, Sandberg G, Ishikawa H, Evans M, and Palme K. 2003. Gravity-regulated differential auxin transport from columella to lateral root cap cells. *Proceedings of the National Academy of Sciences of the United States of America* **100**: 2987–2991.

bioRxiv preprint doi: https://doi.org/10.1101/2020.09.01.277707; this version posted September 2, 2020. The copyright holder for this preprint (which was not certified by peer review) is the author/funder, who has granted bioRxiv a license to display the preprint in perpetuity. It is made available under a CC-BY 4.0 International license.

Patro R, Duggal G, Love MI, Irizarry RA, Kingsford C. 2017. Salmon provides fast and bias-aware quantification of transcript expression. *Nature Methods* **14**: 417–419.

Pernisova M, Prat T, Grones P, Harustiakova D, Matonohova M, Spichal L, Nodzynski T, Friml J, Hejatk J. 2016. Cytokinins influence root gravitropism via differential regulation of auxin transporter expression and localization in Arabidopsis. *New Phytologist* **212**: 497–509.

Potocka I, Szymanowska-Pulka J. 2018. Morphological responses of plant roots to mechanical stress. *Annals of Botany* **122**: 711–723.

Roberts JA, Hussain A, Taylor IB, Black CR. 2002. Use of mutants to study long-distance signalling in response to compacted soil. *Journal of Experimental Botany* **53**: 45–50.

Rowe J, Topping JF, Liu J, Lindsey K. 2016. Abscisic acid regulates root growth under osmotic stress conditions via an. interacting hormonal network with cytokinin, ethylene and auxin. *New Phytologist* **211:** 225-239.

Rutherford R, Masson PH. 1996. *Arabidopsis thaliana sku* mutant seedlings show exaggerated surface-dependent alteration in root growth vector. *Plant Physiology* **111**: 987–998.

Růžička K, Ljung K, Vanneste S, Podhorská R, Beeckman T, Friml J, Benková E. 2007. Ethylene regulates root growth through effects on auxin biosynthesis and transport-dependent auxin distribution. *Plant Cell* **19**: 2197– 2212.

Růžička K, Strader LC, Bailly A, Yang H, Blakeslee J, Łangowski Ł, Nejedlá E, Fujita H, Itoh, H, Syono K, Hejátko J, Gray WM, Martinoia E, Geisler M, Bartel B, Murphy AS, Friml J. 2010. Arabidopsis *PIS1* encodes the ABCG37 transporter of auxinic compounds including the auxin precursor indole-3-butyric acid. *Proceedings of the National Academy of Sciences of the United States of America* **107**: 10749–10753.

Schnittger A, Schoebinger U, Stierhof Y-D, Huelskamp M. 2002. Ectopic B-type cyclin expression induces mitotic cycles in endoreduplicating *Arabidopsis* trichomes. *Current Biology* **12:** 415-420.

Shih HW, Miller ND, Dai C, Spalding EP, Monshausen GB. 2014. The receptor-like kinase FERONIA is required for mechanical signal transduction in Arabidopsis seedlings. *Current Biology* **24**: 1887–1892.

Soneson C, Love MI, Robinson MD. 2016. Differential analyses for RNA-seq: Transcript-level estimates improve gene-level inferences. *F1000 Research* **4**: 1521.

bioRxiv preprint doi: https://doi.org/10.1101/2020.09.01.277707; this version posted September 2, 2020. The copyright holder for this preprint (which was not certified by peer review) is the author/funder, who has granted bioRxiv a license to display the preprint in perpetuity. It is made available under a CC-BY 4.0 International license.

727 **Staswick PE, Serban B, Rowe M, Tiryaki I, Maldonado MT, Maldonado MC, Suza W.**
728 **2005.** Characterization of an arabidopsis enzyme family that conjugates amino acids to
729 indole-3-acetic acid. *Plant Cell* **17**: 616–627.
730 **Strader LC, Chen GL, Bartel B. 2010.** Ethylene directs auxin to control root cell expansion.
731 *Plant Journal* **64**: 874–884.
732 **Supek F, Bošnjak M, Škunca N, Šmuc T. 2011.** Revigo summarizes and visualizes long lists
733 of gene ontology terms. *PLoS ONE* **6**: e21800.
734 **Swarup R, Kramer EM, Perry P, Knox K, Leyser HM, Haseloff J, Beemster GT,**
735 **Bhalerao R, Bennett MJ. 2005.** Root gravitropism requires lateral root cap and epidermal
736 cells for transport and response to a mobile auxin signal. *Nature Cell Biology* **7**: 1057–1065.
737 **Swarup R, Perry P, Hagenbeek D, Van Der Straeten D, Beemster GT, Sandberg G,**
738 **Bhalerao R, Ljung K, Bennett MJ. 2007.** Ethylene upregulates auxin biosynthesis in
739 Arabidopsis seedlings to enhance inhibition of root cell elongation. *Plant Cell* **19**: 2186–
740 2196.
741 **Taylor HM, Ratliff LF. 1969.** Root elongation rates of cotton and peanuts as a function of
742 soil strength and soil water content. *Soil Science* **108**: 113–119.
743 **Topping JF, Lindsey K. 1997.** Promoter trap markers differentiate structural and positional
744 components of polar development in Arabidopsis. *Plant Cell* **9**: 1713–1725.
745 **Veen BW. 1982.** The influence of mechanical impedance on the growth of maize roots. *Plant*
746 *and Soil* **66**: 101–109.
747 **Wang F, Chen ZH, Liu X, Shabala L, Yu M, Zhou M, Salih A, Shabala S. 2019.** The loss
748 of RBOHD function modulates root adaptive responses to combined hypoxia and salinity
749 stress in Arabidopsis. *Environmental and Experimental Botany* **158**: 125–135.
750 **Whalley, WR, Leeds-Harrison PB, Clark LJ, Gowing DJ. 2005.** Use of effective stress to
751 predict the penetrometer resistance of unsaturated agricultural soils. *Soil and Tillage*
752 *Research* **84**: 18–27.
753 **Whalley WR, Watts CW, Gregory AS, Mooney SJ, Clark LJ, Whitmore AP. 2008.** The
754 effect of soil strength on the yield of wheat. *Plant and Soil* **306**: 237–247.
755 **Whitmore AP, Whalley WR. 2009.** Physical effects of soil drying on roots and crop growth.
756 *Journal of Experimental Botany* **60**: 2845–2857.
757 **Wright M, Adams J, Yang K, McManus P, Jacobson A, Gade A, McLean J, Britt D,**
758 **Anderson A. 2016.** A root-colonizing pseudomonad lessens stress responses in wheat
759 imposed by CuO nanoparticles. *PLoS ONE* **11**: e0164635.

bioRxiv preprint doi: https://doi.org/10.1101/2020.09.01.277707; this version posted September 2, 2020. The copyright holder for this preprint (which was not certified by peer review) is the author/funder, who has granted bioRxiv a license to display the preprint in perpetuity. It is made available under a CC-BY 4.0 International license.

Wu F, Chi Y, Jiang Z, Xu Y, Xie L, Huang F, Wan D, Ni J, Yuan F, Wu X, Zhang Y, Wang L, Ye R, Byeon B, Wang W, Zhang S, Sima M, Chen S, Zhu M, Pei J, Johnson DM, Zhu S, Cao X, Pei C, Zai Z, Liu Y, Liu T, Swift GB, Zhang W, Yu M, Hu Z, Siedow JN, Chen X, Pei ZM. 2020. Hydrogen peroxide sensor HPCA1 is an LRR receptor kinase in Arabidopsis. *Nature* **578**: 577–581.

Wu G, Lewis DR, Spalding EP. 2007. Mutations in Arabidopsis multidrug resistance-like ABC transporters separate the roles of acropetal and basipetal auxin transport in lateral root development. *Plant Cell* **19**: 1826–1837.

Xie YJ, Xu S, Han B, Wu MZ, Yuan XX, Han Y, Gu Q, Xu DK, Yang Q, Shen WB. 2011. Evidence of Arabidopsis salt acclimation induced by up-regulation of HY1 and the regulatory role of RbohD-derived reactive oxygen species synthesis. *Plant Journal* **66**: 280–292.

Yamamoto C, Sakata Y, Taji T, Baba T, Tanaka S. 2008. Unique ethylene-regulated touch responses of *Arabidopsis thaliana* roots to physical hardness. *Journal of Plant Research* **121**: 509–519.

Yan J, Wang B, Zhou Y. 2017. A root penetration model of Arabidopsis thaliana in phytagel medium with different strength. *Journal of Plant Research* **130**: 941–950.

Yan J, Wang B, Zhou Y, Hao S. 2018. Resistance from agar medium impacts the helical growth of Arabidopsis primary roots. *Journal of the Mechanical Behavior of Biomedical Materials* **85**: 43–50.

Young IM, Montagu K, Conroy J, Bengough AG. 1997. Mechanical impedance of root growth directly reduces leaf elongation rates of cereals. *New Phytologist* **135**: 613–619.

Zhang R, Calixto, CP, Marquez Y, Venhuizen P, Tzioutziou NA, Guo W, Spensley M, Entizne JC, Lewandowska D, Have ST, Frey NF, Hirt H, James AB, Nimmo HG, Barta A, Kalyna M, Brown JW. 2017. A high quality Arabidopsis transcriptome for accurate transcript-level analysis of alternative splicing. *Nucleic Acids Research* **45**: 5061–5073.

Figure legends

Figure 1. Barrier effects on primary root growth. Seeds were sown in a top layer of 0.3% Phytagel and roots grew for 5mm before encountering the lower media layer. a) Root length of 7 DAG seedlings (Student's *t*-test, $P < 0.001$). b) Distance of root hair emergence from the root

bioRxiv preprint doi: https://doi.org/10.1101/2020.09.01.277707; this version posted September 2, 2020. The copyright holder for this preprint (which was not certified by peer review) is the author/funder, who has granted bioRxiv a license to display the preprint in perpetuity. It is made available under a CC-BY 4.0 International license.

tip of 7 DAG seedlings (Student's *t*-test, $P < 0.001$). c) Meristem length at 7 DAG (Student's *t*-test, $p = 0.79$). d) Elongation zone length at 7 DAG (Student's *t*-test, $P = 0.003$). e) Primary root tip stained with propidium iodide at 7 DAG. Arrowheads indicate quiescent centre and end of the meristematic zone. f) Elongation zone of primary roots stained with propidium iodide. Arrowheads indicate start and end of the elongation zone. Scale bar = 50 µm. g) Mean primary root length between 4-7 DAG when encountering a barrier. For boxplots, upper and lower boundaries of the box indicate the interquartile range (IQR), a black line within the box marks the median, and whiskers represent the min and max excluding outliers. Open circles represent outliers. ns = not significant, * < 0.05, ** < 0.01, *** < 0.001. Error bars indicate mean ± SE.

Figure 2. ROS-related gene expression at 6 h in response to a barrier. a) Venn diagram showing common genes between genes differentially expressed at 6 h in response to a barrier and genes identified as a general ROS transcriptomic footprint (Gadjev *et al*., 2006). b) Number of genes identified from the RNA-Seq data set at 6 h identified by Gadjev *et al*. (2006) as relating to specific reactive oxygen species responses.

Figure 3. ROS is required for the barrier response. a) Timelapse imaging of *atrbohD/F* double mutant in response to a barrier. Plastic barriers were placed in front of 6 DAG vertically growing roots and root tips were imaged every 15 min. b) RTA from 0-360 min] after contact with a barrier. Root tip angle was measured every 15 min. c,d) The effect of diphenylene iodonium (DPI) on root tip angle during the barrier response 6 h after barrier placement. Lines indicate mean and surrounding shaded area indicates ± SE. e-g) HyPer fluorescence in unfixed roots after responding to a barrier. Barriers were placed in front of seedlings 6 DAG and roots were imaged between 3-5 h after barrier placement. Roots were stained with propidium iodide prior to imaging. e) Typical fluorescence of Hyper probe YFP excited at 488 nm (Green) in roots stained with propidium iodide (magenta). f) Measured fluorescence of Hyper YFP in the columella. g) Measured fluorescence of Hyper YFP in root cap border cells.

Figure 4. CellROX staining to reveal ROS levels. Barriers were placed in front of seedlings 6 DAG and seedlings were removed 3 h after barrier placement for staining with CellROX Deep Red. a) Typical staining pattern of CellROX Deep Red (Red) at the root tip. With and without bright field image of the root tip for reference. b) Measured fluorescence of CellROX Deep Red stain in the root tip. c) Typical staining pattern of CellROX Deep Red (Red) in the

bioRxiv preprint doi: https://doi.org/10.1101/2020.09.01.277707; this version posted September 2, 2020. The copyright holder for this preprint (which was not certified by peer review) is the author/funder, who has granted bioRxiv a license to display the preprint in perpetuity. It is made available under a CC-BY 4.0 International license.

827 meristem and elongation zone, with (upper panels) and without (lower panels) bright field
828 imaging. d) Measured fluorescence of CellROX Deep Red stain in the meristem and elongation
829 zone. e) Ratio of CellROX Deep Red fluorescence across the left and right side of the meristem
830 and elongation zone. Ratio was calculated using the formula exp(|(log(left/right))|) to account
831 for any bias in assigning left/right side of the root. Scale bar = 50 µm. Black circles and error
832 bars represent mean ± SE. Coloured circles represent distribution of individual data points.
833 Lines and asterisks show significance (ns = not significant, * < 0.05, ** < 0.01, *** < 0.001).
834
835 **Figure 5. Ethylene signalling is required for the barrier response.** a) Timelapse imaging of
836 wildtype (Col-0, upper panels) and *etr1* (lower panels) between 0 and 8 h after barrier
837 placement. Plastic barriers were placed in front of 6 DAG vertically growing roots and root
838 tips were imaged every 15 minutes. In some cases, *etr1* shows a reversal of growth direction
839 (lower panels at 6 and 8 h). b) RTA from 0-480 minutes after contact with a barrier. Root tip
840 angle was measured every 15 min. The central 'dip' in *etr1* RTA reflects the directional change.
841 Lines and dots indicate mean with shaded area indicating ± SE. Scale bar = 0.5 mm. c) Angle
842 of primary root tips to the horizontal barrier 24 h after barrier placement for wildtype (Col-o)
843 and *etr1*. d,e) Effect of AVG and STS on RTA 6 h (d) and 30 h (e) after barrier placement.
844 Lines indicate mean and surrounding shaded area indicates ± SE. f) Typical root hair growth
845 after 24 hours in the presence or absence of a barrier: untreated (upper panel, in presence of
846 STS (middle panel), in presence of AVG (lower panel). Scale bar represents 500 µm g) Root
847 hair density (number of root hairs/mm root). Root hairs were counted in an approximate 2 mm
848 section of mature root and exact distance measured to calculate root density. h) Root hair
849 length. Root hair length was measured in 20 root hairs within a 2 mm region of root and the
850 average taken to determine root hair length for the sample. Brackets and asterisks indicate
851 significance with a Tukey Pairwise comparison (ns = not significant, * < 0.05, ** < 0.01, ***
852 < 0.001).
853
854 **Figure 6. Ethylene signalling is required for the barrier response.** a) Timelapse imaging of
855 wildtype. (Col-0), *aux1* and *eir1* between 0 and 8 h after barrier placement. Plastic barriers
856 were placed in front of 6 DAG growing roots and root tips were imaged every 15 min. b) RTA
857 over time from 0-480 minutes after contact with a barrier. Root tip angle was measured every
858 15 minutes. Lines and dots indicate mean with shaded area indicating ± SE c) Angle of primary
859 root tips to the horizontal barrier 24 h after barrier placement. d,e) Effect of NPA on RTA
860 during the barrier response 6 h (d) or 24 h (e) after barrier placement. Lines indicate mean and

bioRxiv preprint doi: https://doi.org/10.1101/2020.09.01.277707; this version posted September 2, 2020. The copyright holder for this preprint (which was not certified by peer review) is the author/funder, who has granted bioRxiv a license to display the preprint in perpetuity. It is made available under a CC-BY 4.0 International license.

surrounding shaded area indicates ± SE Scale bar = 0.5 mm. Letters indicate significance with a Tukey Pairwise comparison, $P < 0.05$.

Figure 7. Imaging of reporters reveals auxin distribution changes. Barriers were placed in front of vertically growing roots 6 days after germination (DAG). a) Confocal imaging of the DR5rev::3xVENUS-N7 auxin reporter 6 h after placement of a barrier and stained with propidium iodide before imaging, compared with control. Yellow = Venus, Magenta = propidium iodide. b) Relative mean fluorescence measured using imageJ in the Stele, Columella/Quiescent Centre (QC) and Lateral Root Cap (LRC). c) Confocal imaging of the R2D2 auxin reporter in roots responding to a barrier at 6 h. Green = DII-m3xVenus, Magenta = mDII-ndTomato. Ratiometric image of mDII-ndTomato/ DII-m3xVenus fluorescence produced in imageJ using image calculator. d) Ratio of mDII-ndTomato/ DII-m3xVenus fluorescence. e) Ratio of auxin level across the left and right sides of the root tip. Ratio was calculated using the formula exp(|(log(left/right))|) to account for any bias in assigning left/right side of the root. Scale bar = 50 µm. Black circles and error bars represent mean ± SE. Coloured circles represent distribution of individual data points. Lines and asterisks show significance (ns = not significant, * < 0.05, ** < 0.01, *** < 0.001).

Figure 8. Pathways involved in the root barrier response. Hypotheses generated from results presented throughout the thesis and from previously published literature (numbers). Arrows show hypothesised positive interaction/relationship; t-bars inhibition or negative relationship. Boxed are colour coded according to the source of evidence. Numbers refer to published literature 1. Okamoto *et al*. (2008); Okamoto & Takahashi (2019) 2. Shih *et al*. (2014) 3. Monshausen *et al*. (2009) 4. Gilroy *et al*. (2014, 2016) 5. Růžička *et al*. (2007) 6. Strader *et al*. (2010) 7. Lee *et al*. (2020).

Supporting Information

Figure S1. Barrier systems. a) Magenta pot split layer assay. b) Plastic barrier assay. c) Dialysis membrane barrier assay. d) Root tip angle.

bioRxiv preprint doi: https://doi.org/10.1101/2020.09.01.277707; this version posted September 2, 2020. The copyright holder for this preprint (which was not certified by peer review) is the author/funder, who has granted bioRxiv a license to display the preprint in perpetuity. It is made available under a CC-BY 4.0 International license.

Figure S2. proCYCB1;2::CYCB1:2:GUS expression reveals cell division in impeded roots. a) Typical GUS staining pattern of CYCB1;2:GUS in roots grown in either a single layer of Phytagel (control) or a split layer system consisting of a lower, harder layer to impede growth. b) Number of dividing cells in presence of absence of barrier. c) Ratio of number of dividing cells between the left and right side of the meristem in presence of absence of barrier. Ratio was calculated as exp(|(log(left/right))|). For boxplots, upper and lower boundaries of the box indicate the interquartile range (IQR), a black line within the box marks the median, and whiskers represent the min and max excluding outliers. Open circles represent outliers. Asterisks and brackets indicate significance (ns = not significant, * < 0.05, ** < 0.01). Images and measurement representative of at least 15 samples. Scale bars = 50 µm.

Figure S3. Short-term bending response of a root to a barrier. Plastic barriers were placed in front of 6 DAG growing roots and root tips were imaged every 15 min. a) Time-lapse images of a Col-0 root tip encountering a horizontal barrier at 0-8 h after contact with the barrier. b) Root Tip Angle (RTA) over 0-480 min after contact with a barrier. RTA was measured every 15 minutes. c) Bending rate between 15-480 min. d) Root growth of the primary root tip between 0-480 min after contact with the barrier. Blue line represents Regression line. e) Typical elongation zone of primary root tips stained with Calcofluor White and grown in the presence or absence of a barrier for 6 h. Cells of the elongation zone used for measurements are outlined and highlighted in orange. f) Total cortical cell number in the meristem and elongation zone after 6 h. g) Ratio of meristem and elongation zone length between the left and right side of the root tip. h) Ratio of cell length between the left and right side of the root tip in the first 11 cells of the elongation zone. The root tip was divided through the middle into a left and right side and measurements taken separately for each side. Ratio was calculated using the formula exp(|log(left/right)|) to account for any bias in assigning left/right. Error bars represent mean ± SE. Scale bar = 50 µm.

Figure S4. Analysis of variation in gene expression between and within sample groups. a) Principal component analysis (PCA) plot visualising sample-sample distances. Polygons represent sample groups. PCA performed on regularized logarithm (rlog) transformed data using the R software package DEseq2. b) Clustered Heatmap of rlog transformed count data for the top 50 most highly expressed genes across all samples. Rows and column aggregated using kmeans clustering by the R package pheatmap.

bioRxiv preprint doi: https://doi.org/10.1101/2020.09.01.277707; this version posted September 2, 2020. The copyright holder for this preprint (which was not certified by peer review) is the author/funder, who has granted bioRxiv a license to display the preprint in perpetuity. It is made available under a CC-BY 4.0 International license.

Figure S5. Genes differentially expressed in roots encountering a barrier compared with controls after 6 h and 30 h treatment identified through RNA-Seq. a) Differentially Expressed Genes (DEGs) as estimated by the R software package DEseq2. Red dots represent significant DEGs, black dots non-significant. P-value < 0.05 and a log2 fold change (log2fc) > 0.5 or < - 0.5. b) Significant DEGs separated into up and downregulated genes at the two barrier response timepoints. c) Venn diagram representing overlapping DEGs between treatments.

Figure S6. Treemap output from REVIGO (Supek *et al*., 2011) of genes identified as significantly upregulated (a) and downregulated (b) 6 h after encountering a barrier. P-value < 0.05 and a log2 fold change (log2fc) > 0.5 or < -0.5. Each rectangle represents a gene ontology (GO) term cluster and each colour represents a supercluster of related clusters. Sizes of rectangles reflect the –log10 P-value of each cluster.

Figure S7. Treemap output from REVIGO (Supek *et al*., 2011) of genes identified as significantly upregulated **(a)** and downregulated **(b)** 30 hours after encountering a barrier. P-value < 0.05 and a log2 fold change (log2fc) > 0.5 or < -0.5. Each rectangle represents a gene ontology (GO) term cluster and each colour represents a supercluster of related clusters. Sizes of rectangles reflect the –log10 P-value of each cluster.

Figure S8. Hormone signalling and metabolic/biosynthesis related GO terms identified by GO analysis of genes differentially expressed in response to a barrier. Bar chart showing numbers of DEGs identified by each GO term. Bars are grouped by the hormone the GO term relates to.

Figure S9. Ethylene-related gene expression analysis. a) KEGG Pathway mapping of genes differentially expressed at 6 hours in response to a barrier and identified as being involved in the ethylene signalling pathway. Genes present within the data set are highlighted with colours corresponding to KEGG Orthology (molecular function) definition. b) Genes differentially expressed at 6 hours in response to a barrier and identified as being involved in the ethylene biosynthesis pathway. Components of the pathway with an identified DEG are highlighted red (ACC Synthase), orange (ACC Oxidase) and yellow (ETO1/EOL1).

Figure S10. Response of *etr1* and *ein2* to a barrier. a) Plastic barriers were placed in front of primary roots of seedlings 6 days after germination (DAG) and root tips were imaged at 24

bioRxiv preprint doi: https://doi.org/10.1101/2020.09.01.277707; this version posted September 2, 2020. The copyright holder for this preprint (which was not certified by peer review) is the author/funder, who has granted bioRxiv a license to display the preprint in perpetuity. It is made available under a CC-BY 4.0 International license.

961 hours after encountering a barrier. Scale bar indicates 0.5 mm. b) Angle of primary root tips
962 to the horizontal barrier. Lines indicate mean and surrounding shaded area indicates ± SE.
963 Letters indicate significance with a Tukey Pairwise comparison $P < 0.05$.
964
965 **Figure S11. Growth of *etr1* between 0 and 8 hours after barrier placement.** Root growth
966 as measured by time-lapse imaging of roots encountering a barrier. a) Root growth of the
967 primary root tip between 0-480 min after contact with the barrier. b) Root growth rate
968 (µm/min) between 15-480 min after encountering a barrier. Plastic barriers were placed in
969 front of 6 day old vertically growing roots and root tips were imaged every 15 min. Lines and
970 dots indicate mean with shaded area indicating ± SE. Letters indicate significance after a
971 *Student's* t-test (*** < 0.001).
972
973 **Figure S12. Growth of wildtype and ethylene-sensitive mutant roots after barrier**
974 **placement.** Primary root length was measured after growth of seedlings on dialysis membrane
975 barriers for 7 days post germination. Error bars represent standard error of the mean of 15
976 seedlings per treatment. Root growth of the mutants was not significantly inhibited by barrier
977 impedance (ANOVA and Tukey pairwise comparison, *** = P <0.0001, ** = P <0.001).
978
979 **Figure S13. KEGG Pathway mapping of genes differentially expressed at 6 and 30 hours**
980 **in response to a barrier and identified as being involved in the auxin signalling pathway.**
981 Genes present within the data set are highlighted with colours corresponding to KEGG
982 Orthology (molecular function) definition.
983
984 **Figure S14. Confocal imaging of R2D2 in roots responding to a barrier between 0-4 h**.
985 Barriers were placed in front of root tips 6 DAG. a) R2D2 fluorescence at the root tip at 0-4 h
986 with accompanying ratio metric image of generated from mDII-ndTomato/ DII-m3xVenus
987 fluorescence using ImageJ. For ratiometric images calibration bar indicates mean grey value.
988 b) Ratio of mDII-ndTomato/ DII-m3xVenus fluorescence. c) Ratio of auxin level across the
989 left and right sides of the root tip. Scale bar = 50 µm. Black circles and error bars represent
990 mean ± SE. Coloured circles represent distribution of individual data points. Letters indicate
991 significant difference after post-hoc TUKEY test, $P < 0.05$.
992
993 **Supplemental Table 1.** NADPH-oxidase genes identified through RNA-Seq that are
994 upregulated during the barrier response at 6 hours.

bioRxiv preprint doi: https://doi.org/10.1101/2020.09.01.277707; this version posted September 2, 2020. The copyright holder for this preprint (which was not certified by peer review) is the author/funder, who has granted bioRxiv a license to display the preprint in perpetuity. It is made available under a CC-BY 4.0 International license.

995

996 **Supplemental Table 2.** List of genes that act as reactive oxygen species (ROS) scavengers
997 identified in the RNA-Seq data of differentially expressed genes in response to a barrier log2fc
998 identified with P-value <0.05.

999

bioRxiv preprint doi: https://doi.org/10.1101/2020.09.01.277707; this version posted September 2, 2020. The copyright holder for this preprint (which was not certified by peer review) is the author/funder, who has granted bioRxiv a license to display the preprint in perpetuity. It is made available under a CC-BY 4.0 International license.

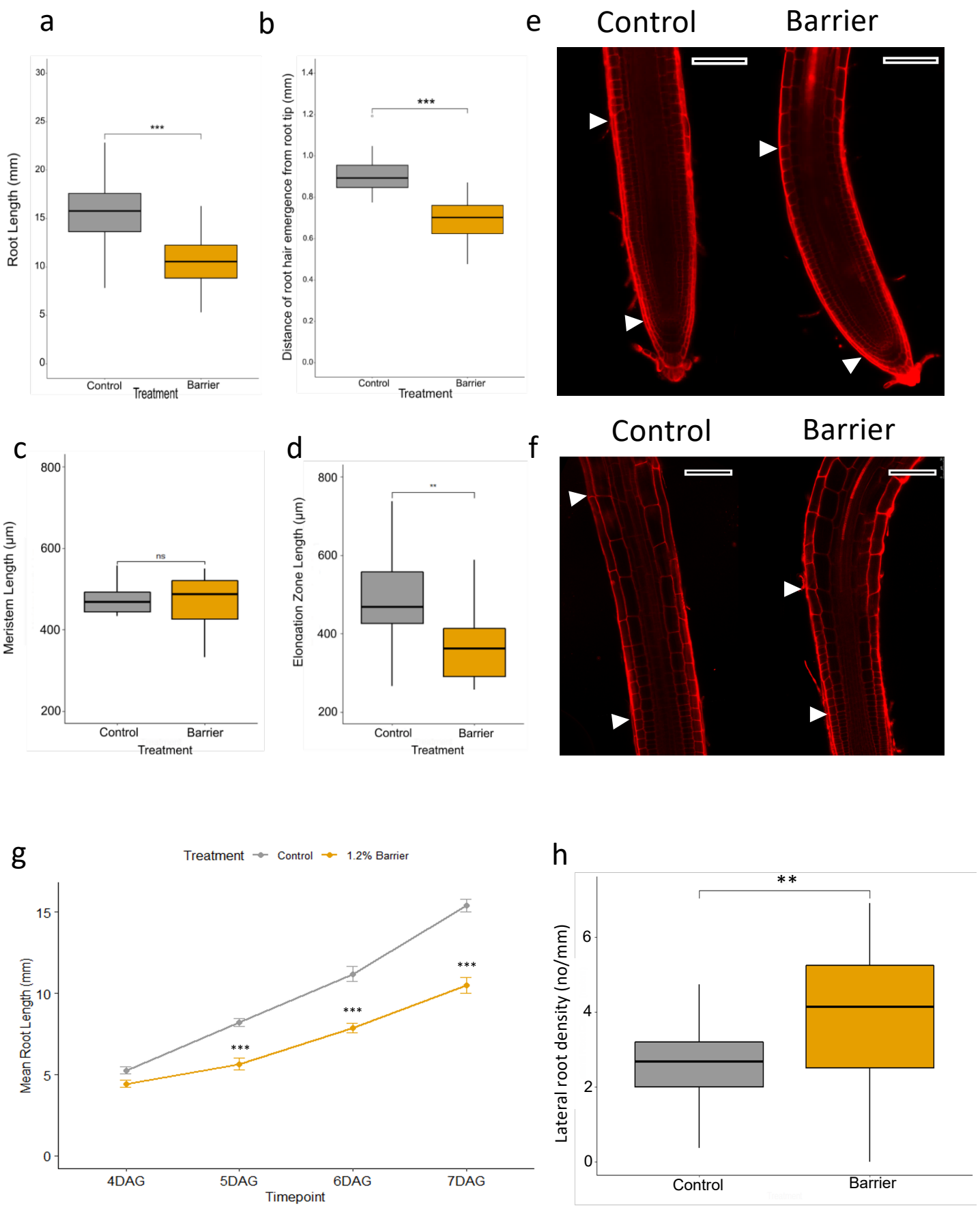


Fig. 1

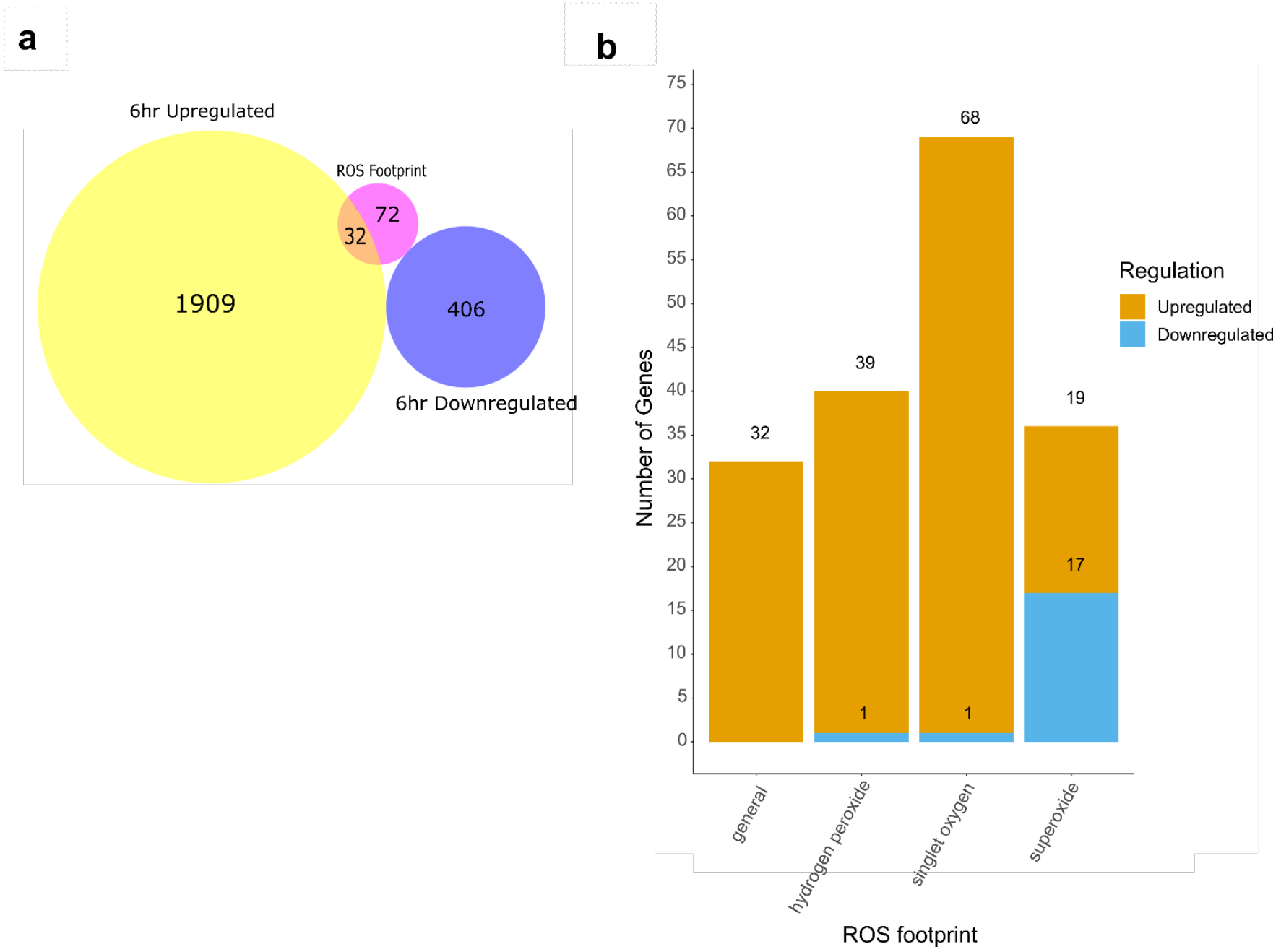

a
6hr Upregulated
ROS Footprint
72
32
1909
406
6hr Downregulated
b
Number of Genes
75
70
65
60
55
50
45
40
35
30
25
20
15
10
5
0
68
39
32
19
17
1
1
Regulation
Upregulated
Downregulated
general
hydrogen peroxide
singlet oxygen
superoxide
ROS footprint

Fig. 2

bioRxiv preprint doi: https://doi.org/10.1101/2020.09.01.277707; this version posted September 2, 2020. The copyright holder for this preprint (which was not certified by peer review) is the author/funder, who has granted bioRxiv a license to display the preprint in perpetuity. It is made available under a CC-BY 4.0 International license.

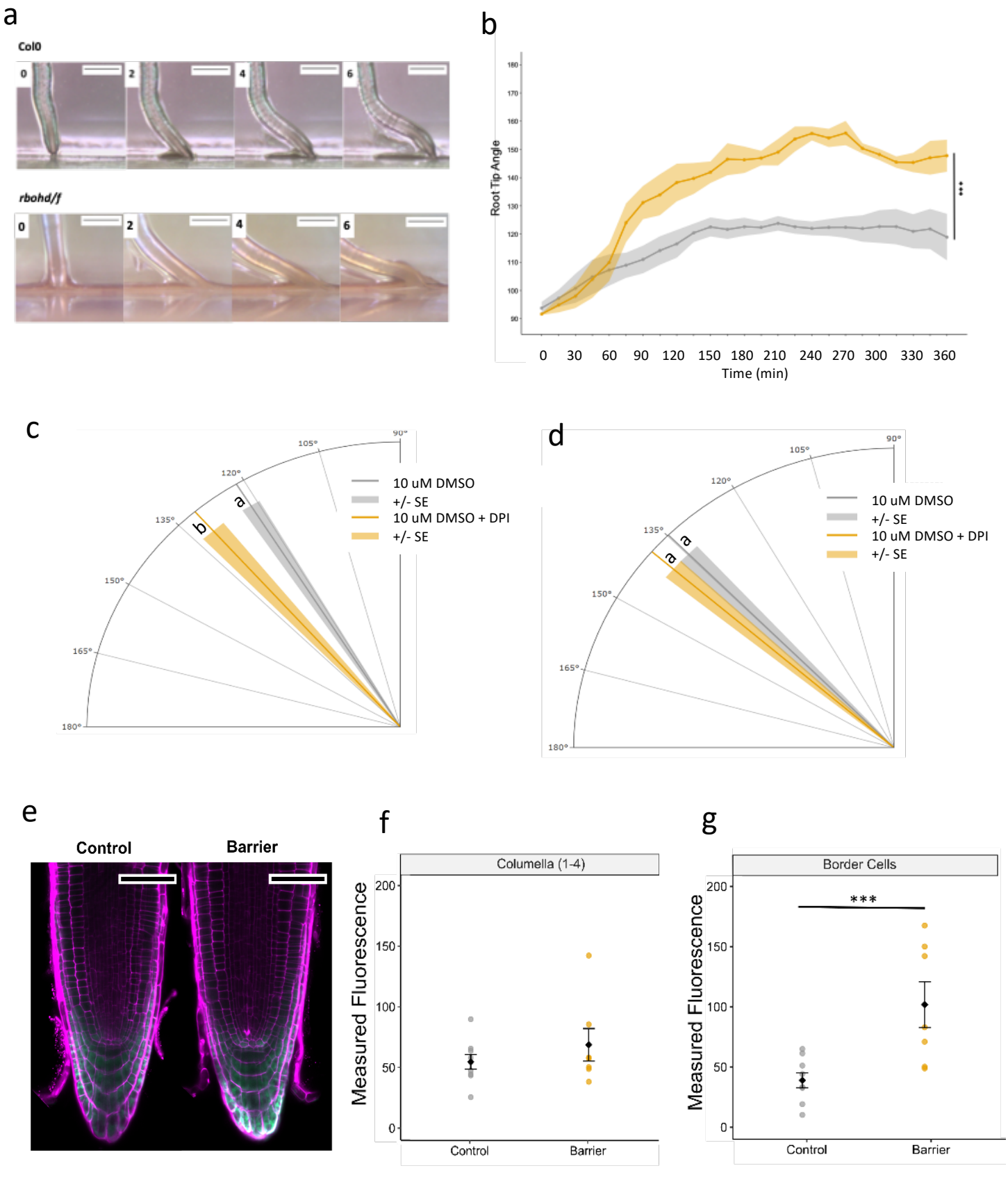


Fig. 3

bioRxiv preprint doi: https://doi.org/10.1101/2020.09.01.277707; this version posted September 2, 2020. The copyright holder for this preprint (which was not certified by peer review) is the author/funder, who has granted bioRxiv a license to display the preprint in perpetuity. It is made available under a CC-BY 4.0 International license.

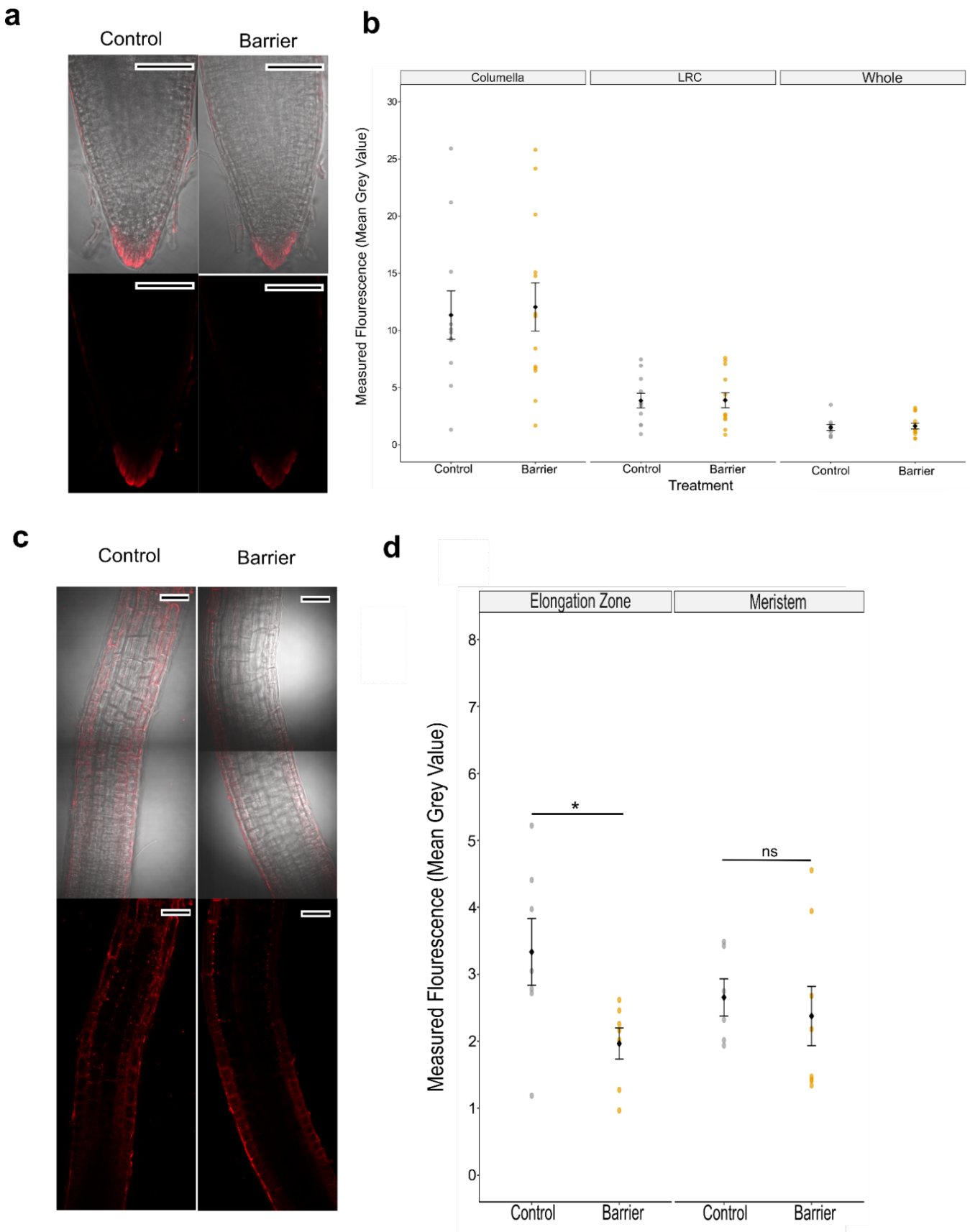


Fig. 4

bioRxiv preprint doi: https://doi.org/10.1101/2020.09.01.277707; this version posted September 2, 2020. The copyright holder for this preprint (which was not certified by peer review) is the author/funder, who has granted bioRxiv a license to display the preprint in perpetuity. It is made available under a CC-BY 4.0 International license.

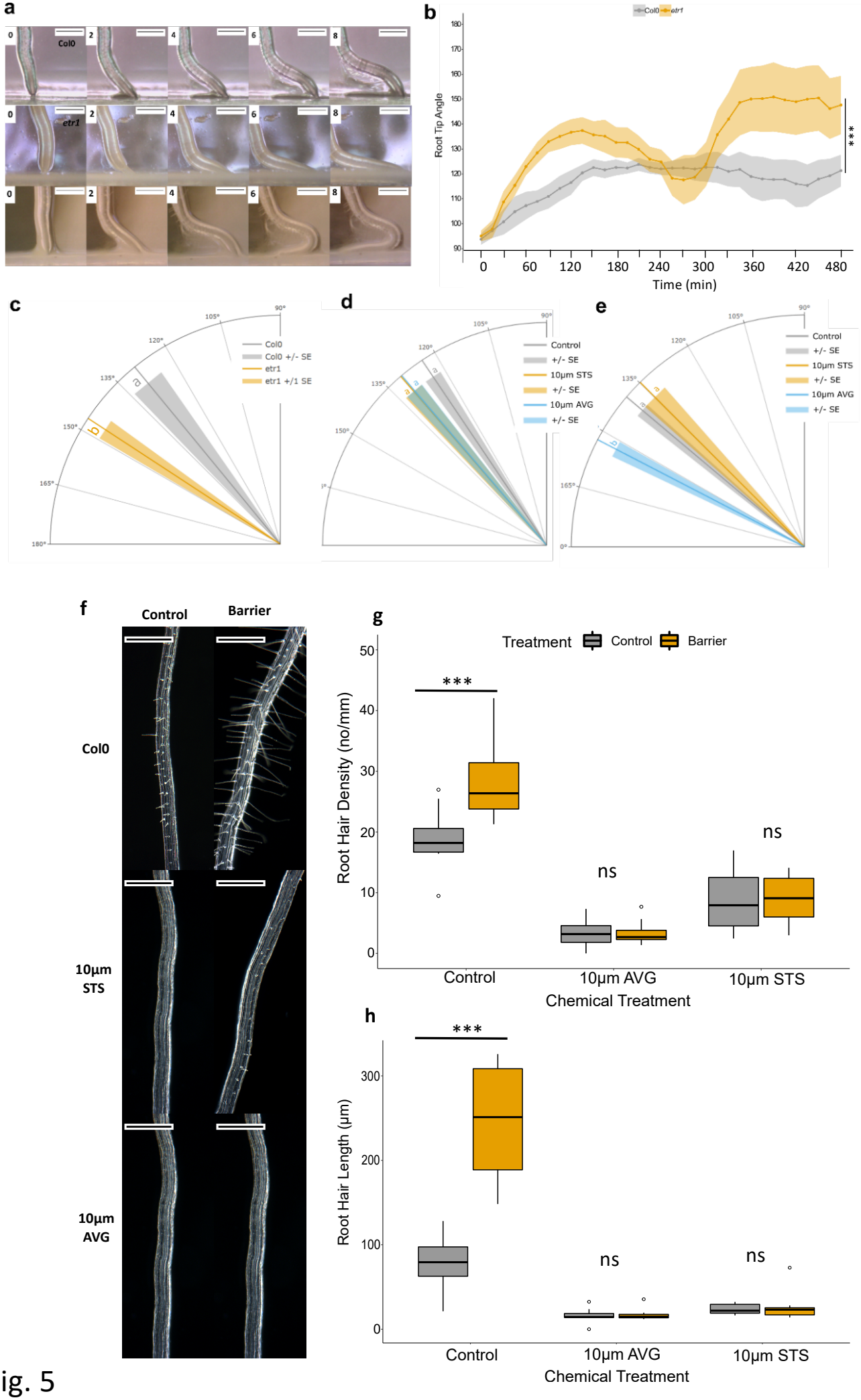


Fig. 5

bioRxiv preprint doi: https://doi.org/10.1101/2020.09.01.277707; this version posted September 2, 2020. The copyright holder for this preprint (which was not certified by peer review) is the author/funder, who has granted bioRxiv a license to display the preprint in perpetuity. It is made available under a CC-BY 4.0 International license.

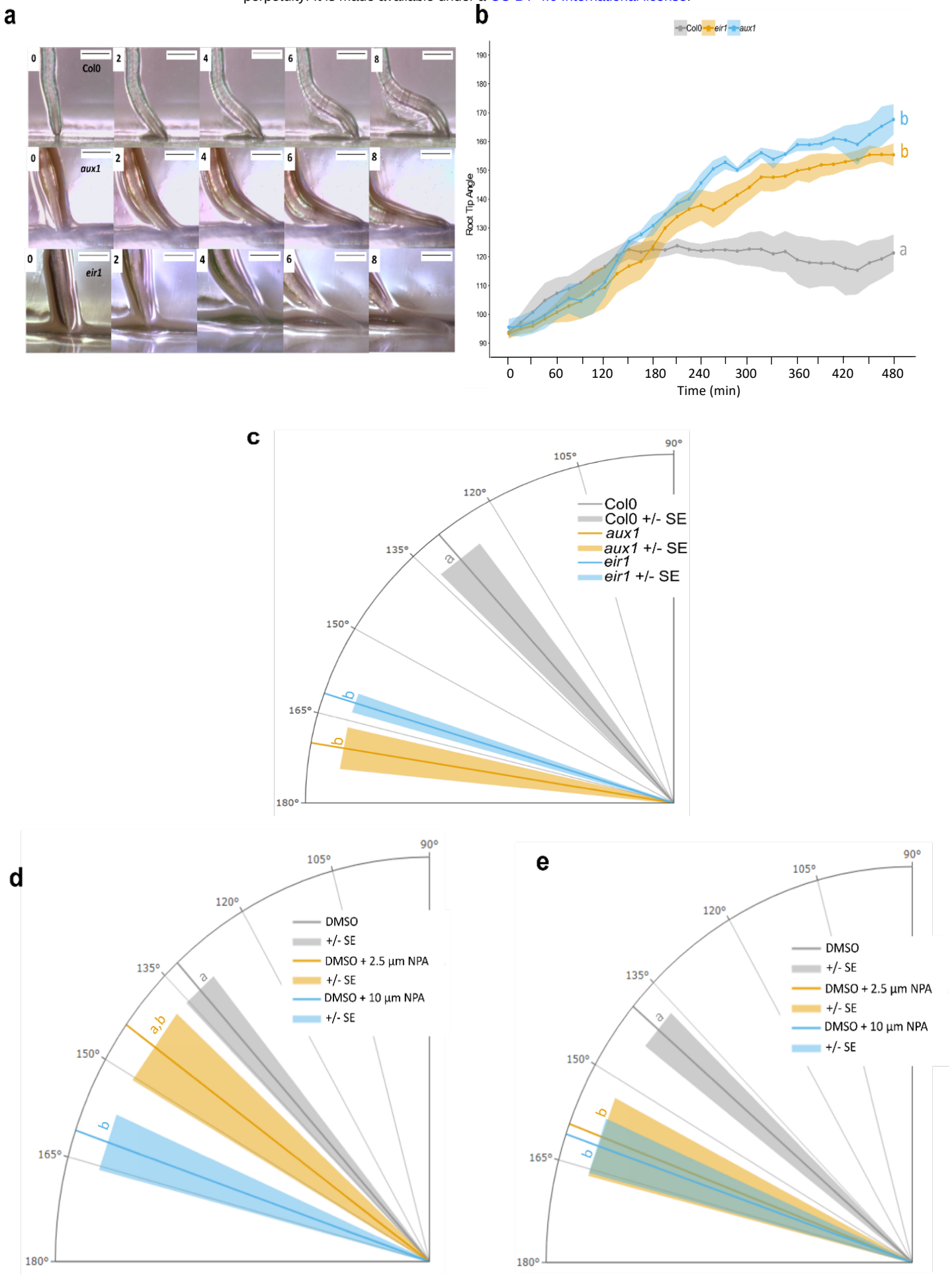


Fig. 6

bioRxiv preprint doi: https://doi.org/10.1101/2020.09.01.277707; this version posted September 2, 2020. The copyright holder for this preprint (which was not certified by peer review) is the author/funder, who has granted bioRxiv a license to display the preprint in perpetuity. It is made available under a CC-BY 4.0 International license.

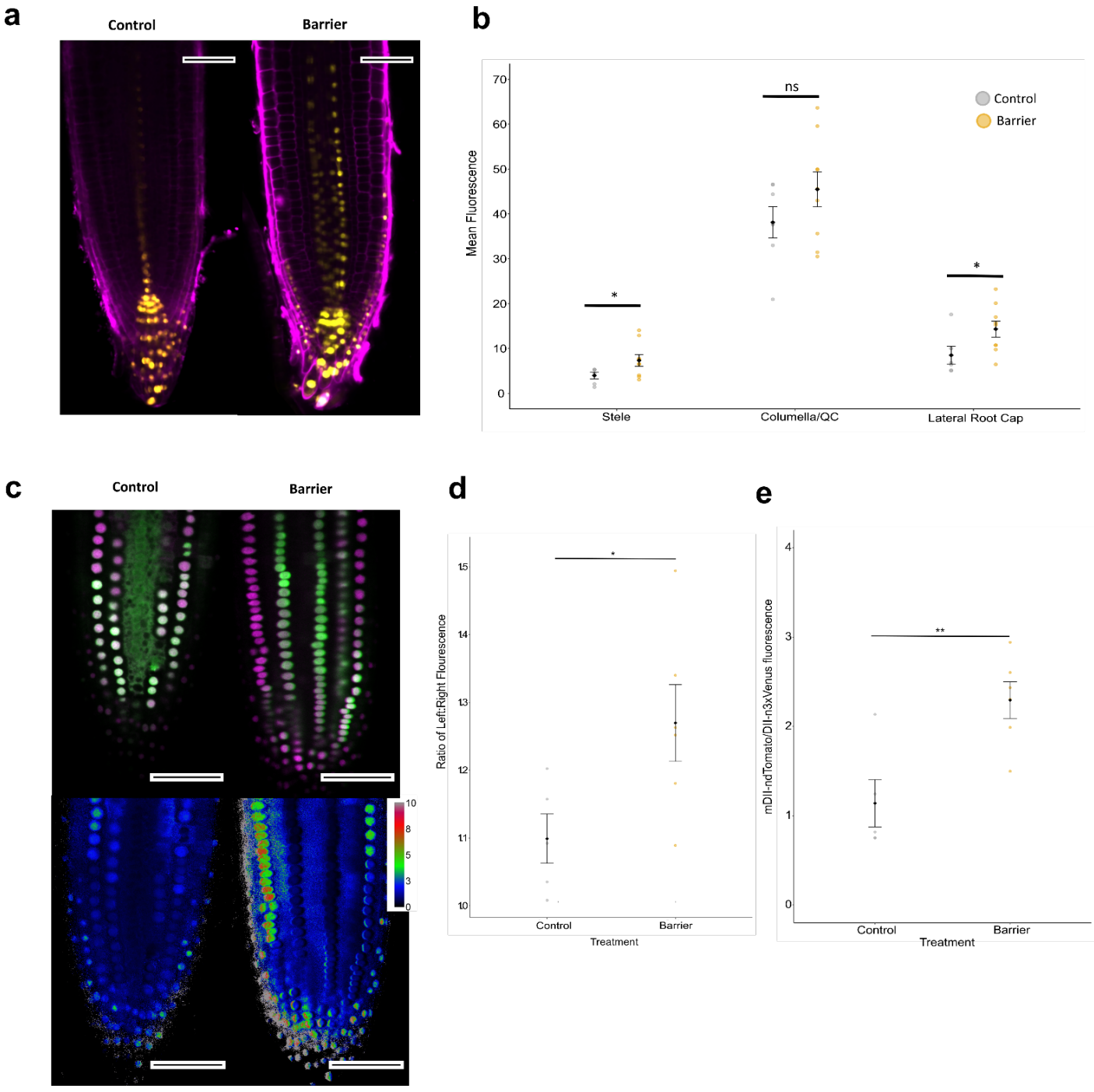


Fig. 7

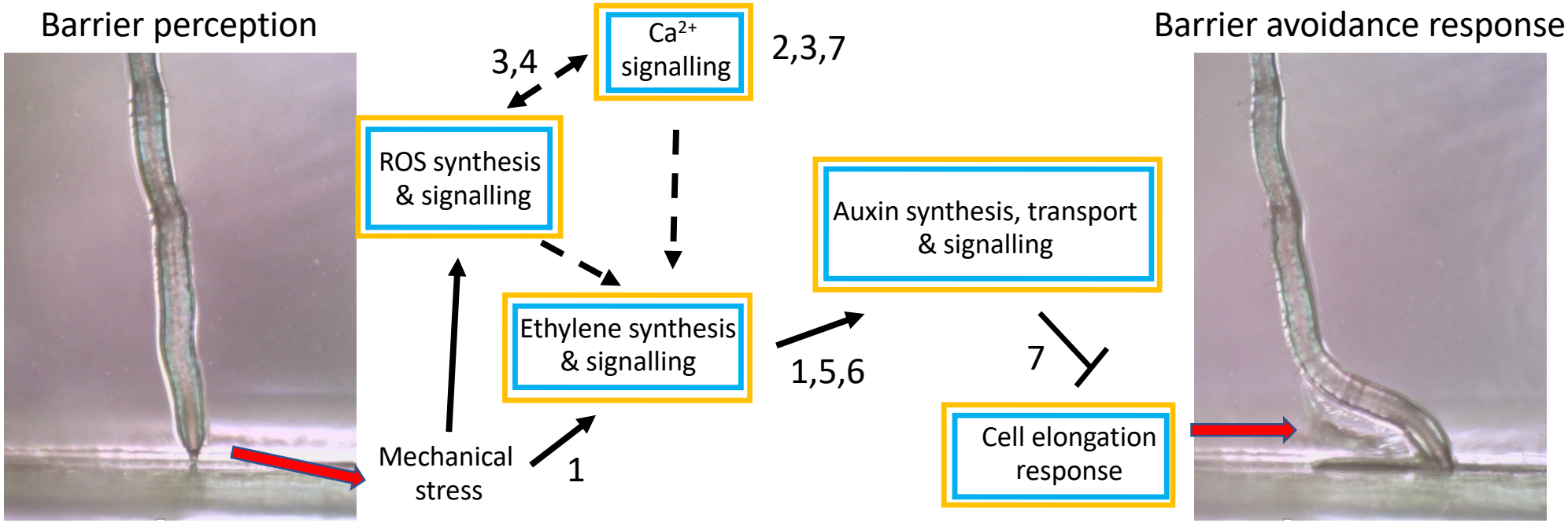

Barrier perception
Barrier avoidance response
Ca2+ signalling
3,4
2,3,7
ROS synthesis & signalling
Auxin synthesis, transport & signalling
Ethylene synthesis & signalling
1,5,6
7
Cell elongation response
Mechanical stress
1
Evidence from literature
Evidence from this paper – RNA-seq/experimental
Interaction hypothesized but not confirmed experimentally
Interaction confirmed experimentally

Fig. 8